Progress in Oceanography 244 (2026) 103723

Contents lists available at ScienceDirect

Progress in Oceanography

journal homepage: www.elsevier.com/locate/pocean

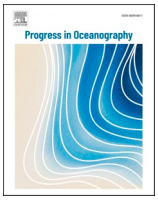

Skillful high-resolution seasonal forecasts of the California Current System using model-analogs

Dillon J. Amaya [a,*], Michael G. Jacox [a,b], Michael A. Alexander [c]

[a] Physical Science Laboratory, National Oceanic and Atmospheric Administration, 325 Broadway, Boulder, CO 80305, USA
[b] Ecosystem Science Division, Southwest Fisheries Science Center, National Oceanic and Atmospheric Administration, 99 Pacific St #255A, Monterey, CA 93940, USA
[c] Department of Atmospheric and Oceanic Sciences, University of Colorado Boulder, Boulder, CO, USA

ARTICLE INFO

Keywords:
Ocean prediction
California Current System
Seasonal forecasting
High-resolution climatemodeling
ENSO
Model-analogs

ABSTRACT

Despite recent advances in the development of seasonal forecasting systems, high-resolution climate modeling in support of operational prediction efforts remains a computational challenge. Here, we use the model-analog technique to overcome computational bottlenecks associated with model resolution and data availability, generating a suite of high-resolution (0.1°) ocean reforecasts at 1–12 months lead from an existing high-resolution global climate simulation—CESM-HR. In our model-analog framework, we compare past observed climate states to the CESM-HR data library (i.e., model sea surface temperature output), with the best matches retained as "analogs". The subsequent model evolution of each analog is then treated as a forecast. We show that high-resolution model-analog (HR-MA) ocean forecasts in the California Current System (CCS) are comparable to the skill of similar high-resolution initialized forecasts derived from a regional model. Forecasts of sea surface temperature, sea surface height, and bottom temperature are particularly skillful, with significant skill above persistence at ~6–10 month leads when forecasting boreal winter. By selecting analogs based on different regions, we further show that seasonal predictability in the CCS is primarily driven by ENSO and month-to-month persistence. Finally, we show that, in an absolute sense, HR-MA forecasts are generally more skillful than low-resolution (1°) model-analog forecasts at predicting coastal conditions throughout the CCS. However, both high- and low-resolution analog forecasts similarly capture the observed timing of nearshore CCS variability, suggesting that even relatively coarse resolution models could provide useful management support tools. Our research highlights model-analogs as a cost-effective method for generating skillful, high-resolution seasonal climate forecasts in support of operational management strategies.

1. Introduction

Seasonal climate forecasts provide important decision support tools to help stakeholders manage a variety of socioeconomically-relevant resources. For example, initialized dynamical forecasts are routinely used to provide seasonal outlooks of regional precipitation and surface temperature, tropical cyclone activity, and climate modes such as the El Niño-Southern Oscillation (ENSO). Currently, these outlooks are most often generated using climate models run at relatively coarse horizontal resolutions, usually with ~ 1° grid spacing. While coarse resolution seasonal forecasts are extremely useful for a wide-variety of applications (e.g., Becker et al., 2022), there is a growing desire for finer-scale climate forecasts and projections that capture the regional dynamics most relevant for local management strategies. With recent advances in computational resources, modeling centers have thus begun to explore the potential benefits of high-resolution (0.25° or less) coupled climate modeling to support decision making based on more granular climate information.

Recent research has shown that finer resolution models more accurately capture many key aspects of the climate system, including the strength of ocean–atmosphere coupling, the strength and position of the storm tracks, the sign and intensity of Pacific decadal trends, large-scale ocean circulation, and mesoscale ocean variability (e.g., Chang et al., 2020; Drenkard et al., 2021; Meehl et al., 2019). While climate forecasts based on high-resolution global models have also been shown to be more accurate than their low-resolution counterparts (Infanti & Kirtman, 2019; Kim et al., 2023; Siqueira et al., 2021; Yeager et al., 2023; Zhang et al., 2024), developing and maintaining high-resolution operational

* Corresponding author.
E-mail address: dillon.amaya@noaa.gov (D.J. Amaya).

https://doi.org/10.1016/j.pocean.2026.103723
Received 26 June 2025; Received in revised form 26 January 2026; Accepted 10 March 2026
Available online 15 March 2026
0079-6611/Published by Elsevier Ltd.

forecast systems remains challenging due to the significant computational demands of simulating the coupled climate system at resolutions finer than ~100 km. There are, however, different techniques that can reduce the computational costs associated with high-resolution climate forecasting. For example, several studies have generated skillful seasonal ocean forecasts at 1.5 km-10 km resolution by forcing a regional ocean model with output from a traditional coarse resolution global climate model (Jacox et al., 2023; Kearney et al., 2021; Ross et al., 2024; Siedlecki et al., 2016). Others have leveraged nested high-resolution grids within a global coarse resolution model (e.g., Lin et al., 2024; Wills et al., 2024). Still, while regional and nested models may improve the representation of fine-scale features within a given domain, these simulations do not necessarily improve the representation of predictable interannual variability, which arises primarily from large-scale variability (e.g., ENSO teleconnections). For example, statistical downscaling to improve the spatial representation of atmospheric forcing improved biases in a regional ocean forecast but not anomaly forecast skill (e.g., Jacox et al. 2023). Additionally, despite requiring fewer computational resources than a global high-resolution model, regional model forecasts are often still limited in terms of the number of times they are initialized each year, the size of the forecast ensemble, and the length of the reforecast period (i.e., forecasts of the past, using information that was only available at the time of initialization) used to evaluate model skill.

One forecasting technique that has the potential to overcome the computational bottlenecks associated with high-resolution climate forecasting is the "model-analog" approach. In the traditional analog framework, past observed climate states are compared to the current state and the subsequent evolution of the closest matches (or analogs) are treated as forecasts (Lorenz, 1969). Ding et al. (2018) recently built upon this method, expanding the "library" of possible analog climate states to include coupled climate model simulations, with the model evolution treated as the forecast. Drawing analogs from lengthy pre-industrial control simulations resulted in closer matches with observation and allowed for the generation of forecast ensembles, leading to overall more accurate predictions. Following these developments, the model-analog technique has since been shown to produce seasonal climate forecasts that are as skillful as those from initialized dynamical forecasts (Ding et al., 2019, 2018; Ding and Alexander, 2023; Lou et al., 2025, 2023; Menary et al., 2021) with several added benefits:

1. Model-analog forecasting is computationally efficient. In particular, by leveraging existing climate model simulations, model-analogs essentially eliminate the sustained computational cost of producing real-time forecasts using traditional model initialization methods. Therefore, there are virtually no limitations on the number of initializations each year, the forecast ensemble size, or the reforecast length. Additionally, once an analog is identified, the evolution of any model variable can be treated as a forecast (e.g., Ding et al. 2019), allowing for detailed analysis of variables not typically prioritized by operational modeling centers.
2. The computational efficiency of model-analogs overcomes issues related to data storage, as model-analog forecasts can be easily and quickly reproduced, thus eliminating the need to provide long-term storage for vast amounts of high-resolution model output. Although, ample storage for the parent data library is required.
3. Since model-analogs are not truly initialized with observations as in dynamical forecasts (e.g., with data assimilation), analog forecasts already exist in the biased model state. As a result, model-analogs do not drift over the length of forecast, thus avoiding potential forecast errors related to "initialization shock".

Here, we apply the model-analog technique to generate a suite of 0.1° (~10 km) seasonal reforecasts of the California Current System (CCS), based on analogs drawn from a high-resolution version of the Community Earth System Model (CESM). Specifically, we evaluate the skill of model-analog reforecasts of the ocean state along the US west coast out to 12-months lead from 1994 to 2019, with direct comparisons to an existing high-resolution initialized forecast based on a regional ocean model. Although the analog method can be used to forecast any region/domain, we primarily focus on ocean forecasts in the CCS for three main reasons: 1) As an upwelling system, the CCS features disproportionately high primary productivity and fish catch (e.g., Chavez & Messié, 2009) and thus provides habitat to a wide variety of sensitive marine ecosystems whose management would benefit from high-resolution, forward-looking environmental information (Cannizzo and Selz, 2021; Jacox et al., 2023; Tommasi et al., 2017), 2) Dynamically downscaled reforecasts of the CCS exist for direct comparison (Jacox et al. 2023), and 3) While there has been substantial progress in ocean forecasting in recent years, bottlenecks associated with climate model resolution and the availability of oceanographic output still exist (Minobe et al., 2022). In particular, operational forecasting models are often too coarse to accurately represent the coastline and the finer scale features known to influence marine ecosystems. Additionally, while high-resolution alternatives based on regional models may feature a full suite of oceanography output, they often have limited initializations throughout the calendar year. Therefore, high-resolution model-analog forecasts of the CCS provide a unique opportunity to explore the predictability of the ocean more thoroughly than is possible with other currently available datasets.

2. Data and methods

2.1. High-resolution model-analog forecasts

High-resolution model-analog (HR-MA) reforecasts are drawn from a high-resolution version of CESM1.3 (CESM-HR), which features global 0.25° atmosphere and land models and a 0.1° ocean model (Chang et al., 2020). The model climate forcing is set to pre-industrial (1850) conditions and kept constant for 500-years, though the first 150 years are unusable due to a hardware issue identified during model integration (Zhang et al., 2020). Therefore, we only use the last 350 years (model years 170–519) to produce HR-MA forecasts, which also serves as the base period for anomaly calculations. Note that we also attempt to remove any model drift in CESM-HR by first removing the linear trend across the full record for all model variables prior to analysis. See Chang et al. (2020) for more details on CESM-HR.

The reforecast period for our analysis is January 1994-December 2019, which is when we have the most reliable and comprehensive high-resolution observations to verify our forecasts against (see Section 2.3). During this time period, analogs are selected by comparing the sea surface temperature anomalies (SSTAs) from the NOAA Optimum Interpolation Sea Surface Temperature version 2.1 (OISSTv2.1; Huang et al., 2021; Reynolds et al., 2007) dataset to those in CESM-HR. As such, observed SSTAs are relative to a long-term climatology of 1994–2019 and are linearly detrended at each grid cell. The observations were detrended in order to more fairly compare to the CESM-HR pre-industrial simulation, which does not have radiatively forced trends. Results are consistent when selecting analogs without first detrending observations (not shown). The CESM-HR SSTAs are regridded to the OISSTv2.1 0.25° × 0.25° grid prior to comparison. Model-analog forecasts are then generated using the following steps (see also schematic Fig. 1):

(1) Data library: We first generate a data library of possible analog matches by extracting global maps of monthly mean SST from CESM-HR and removing the long-term monthly mean climatology at each grid cell. Our focus is on 12-month forecasts; therefore, the data library for each calendar month consists of 349 possible matches (e.g., all the Januarys from years 170–518 in CESM-HR).

(2) Selecting analogs: For a given month, we choose analogs by minimizing the total distance (*d*) between the observed SSTAs and those from the corresponding CESM-HR monthly data library (i.e., by comparing an observed January to the January data library). While

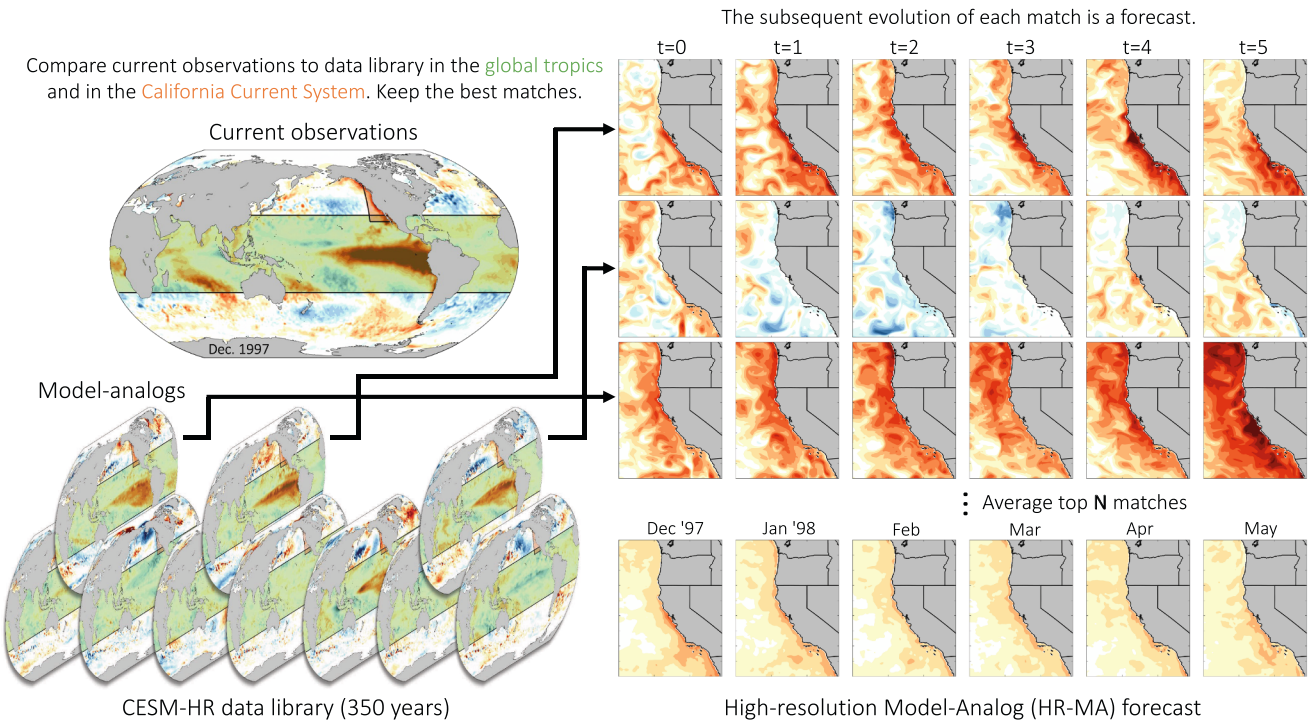

Fig. 1. Schematic illustration of the high-resolution model-analog (HR-MA) method. Analogs are selected by minimizing the difference between observed SSTAs in a given month (e.g., December 1997 in this example) and those from the 350-year pre-industrial control simulation from CESM-HR in the global tropics (green shading) and the California Current System (orange shading). Once analogs are identified, their subsequent evolution in the model is treated as a forecast. The top *N* matches are then averaged to generate an ensemble mean HR-MA forecast for a given variable.

there are many different methods for estimating the distance between two climate states, we use the root mean squared difference (RMSD) of SSTAs in two domains, the global tropics from 30°S-30°N (Fig. 1; green region) and the CCS from 25°N-55°N, 130°W-110°W (Fig. 1; orange region):

$$d = RMSD_{Tropics} + RMSD_{CCS} \quad (1)$$

where RMSD in a given region is defined as:

$$RMSD = \left(\frac{\sum_{i=1}^{I} cos\phi_i \left(\frac{x_i}{\sigma_x} - \frac{y_i}{\sigma_y} \right)^2}{\sum_{i=1}^{I} cos\phi_i} \right)^{\frac{1}{2}} \quad (2)$$

Here, i represents all horizontal spatial grid points, ϕ is the latitude, x is the observed initial state from OISSTv2.1, and y represents each state in the CESM-HR library. The terms σ_x and σ_y denote the square-root of the domain-averaged variance (i.e., the temporal variance at each grid cell, averaged over the domain) within a respective input region (i.e., either the global tropics or the CCS) and are used for standardization purposes. Eq. (1) is similar to the distance metrics used by Ding et al. (2018) and Toride et al. (2025), but modified to incorporate two matching regions. Once calculated, the distances are then ranked in increasing order, with the top 20 closest matches retained from the data library to create a forecast ensemble.

(3) Forecast interpretation: Upon identifying the best model-analogs for a given month, we generate the HR-MA forecast ensemble by following the subsequent 13-month evolution of the CCS in each respective match using the original 0.1° CESM-HR dataset. The 13-month forecast corresponds to lead times of 0-months (i.e., the "initialization" month) to 12-months. These lead times mimic the real-time deployment of the model-analog method, where each monthly initialization is based on the prior month's observations. For example, a HR-MA forecast generated on January 1 is created by comparing December CESM-HR data to observed monthly mean SSTAs in the prior December. In this scenario, the December forecast is the analog match and represents 0-months lead, while the following January, February, and March represent 1-, 2-, and 3- months lead, and so on. See Fig. 1 (and/or Fig. 7 in Ding et al. 2018) for a schematic interpretation of the HR-MA lead times.

While we only use SSTAs to identify analogs in CESM-HR, we are not limited to only SSTA forecasts for analysis. Once the closest SSTA state is identified, the evolution of any model variable can be treated as a forecast (e.g., Ding et al. 2019). In this way, we assess the forecast skill of monthly mean anomalies of SST, sea surface height (SSH), bottom temperature (BT) in regions with bottom depths shallower than 1000 m, stratification as measured by the buoyancy frequency (BF) averaged over the upper 200 m of the water column, the mixed layer depth (MLD) defined by a potential density change of 0.125 kg/m^{-3}, surface currents in the zonal (SU) and meridional (SV) directions, surface wind stress in the zonal (Taux) and meridional (Tauy) directions, and wind stress curl (Curl). These variables were selected as they are commonly used to predict the distribution of marine species ranging from phytoplankton and krill (Anderson et al., 2019; Cimino et al., 2020) to fish, sharks, and top predators (e.g., Abrahms et al., 2019; Brodie et al., 2018).

In addition to the above ocean variables, we evaluate the forecast skill of two indicators of ecological conditions in the CCS, the Habitat Compression Index (HCI; Santora et al., 2020; Schroeder et al., 2022) and the Temperature Observations to Avoid Loggerhead Turtles tool (TOTAL; Welch et al., 2019). The HCI measures the extent of cool, productive waters nearshore. Periods of habitat compression increase the risk that whales will venture closer to shore in search of prey, thereby increasing their risk of entanglement in fishing gear. It is calculated as the number of grid cells with SST lower than a monthly SST threshold within 150 km of the coastline from 35°N-40°N (Fig. 2a; blue line), normalized by the total number of grid cells in that domain. The monthly SST thresholds are the long-term monthly mean SST averaged from the coast to 75 km offshore in the same region. See Schroeder et al. (2022) and Brodie et al. (2023) for more details. The TOTAL tool monitors SSTA in the Southern California Bight (31°N-34°N, 120°W-116°W)

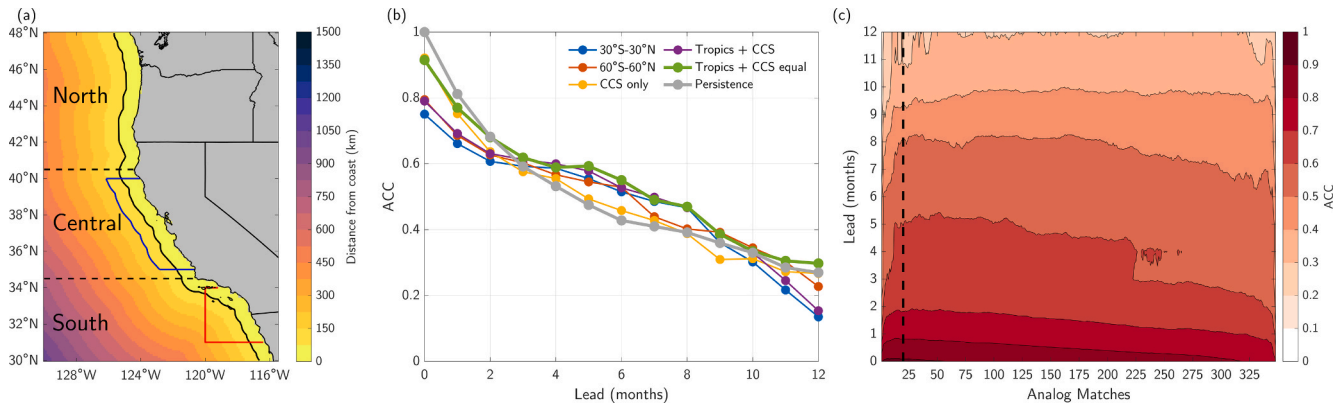

Fig. 2. (a) The California Current System (CCS) regional forecast domain. Shading is the distance of each 0.1° ocean grid cell in CESM-HR from the nearest land grid cell. Black contour marks 75 km from shore. The dashed lines separate the North, Central, and South coastal subregions used in Fig. 5. Blue contour marks the region within 150 km of land that is used to calculate the HCI. Red contour denotes the region used to calculate the TOTAL tool. (b) Ensemble mean skill across all initialization months for different HR-MA SSTA forecasts averaged within 75 km of the US west coast. Different line colors denote different matching regions that were used to select the respective analogs. Gray indicates persistence forecast skill. Here, skill is based on 10 member ensembles for each respective analog selection criteria. (c) Ensemble mean skill of HR-MA SSTA forecasts averaged within 75 km of the US west coast as a function of ensemble size (i.e., how many analog matches are retained). Here, skill is for analogs selected using both tropical and CCS differences, equally weighted (i.e., Eq. (1)); green line in panel b). The dashed line in (c) highlights the skill of the top 20 analogs, which is the HR-MA configuration used for most of our analysis.

and produces alerts when elevated temperatures increase bycatch risk for loggerhead sea turtles (*Caretta caretta*) in June, July, or August. TOTAL is calculated using 6-month running mean SSTAs averaged in the Southern California Bight (Fig. 2a; red line), with alerts issued based on the SSTA of the preceding six months. As a result, there are six possible lead times for each closure month given a 12-month forecast. For example, for a potential June 2026 closure, TOTAL forecasts could be generated as early as May 2025 (e.g., 12-months lead) to December 2025 (e.g., 6-months lead). See Welch et al. (2019) and Brodie et al. (2023) for more details.

2.2. High-resolution model-analog sensitivities

There are several seemingly arbitrary choices that must be made when adapting the model-analog forecasting technique. First, we chose to select analogs by minimizing the distance between observations and CESM-HR in the global tropics and in the CCS, weighting those regional differences equally (Eq. (1)). We have tested other matching domains (30S-30N, 60S-60N, CCS-only, and CCS + tropical unequally weighted) and found that Eq. (1) yields the highest nearshore SST forecast skill for most lead times (Fig. 2b; green line). The impact of matching domain on HR-MA forecast skill will be explored in more detail in Section 3.3.

Second, we chose to keep the top 20 analogs to construct our HR-MA forecast ensemble for each variable. Selecting the number of analogs is a balance between maximizing the deterministic climate signals that are shared among the best matches and increase forecast skill, while not diluting the forecast with poor matches that are far from the observed climate state and decrease forecast skill. We have tested every possible combination of HR-MA ensemble size and found that forecast skill peaks starting around 20 members before leveling off for larger ensemble sizes (Fig. 2c).

Third, while we chose to select analogs based on comparisons to observed SSTAs, studies have shown that the addition of other climate anomalies (e.g., SSHA) in the matching criteria can improve the quality of the analog and lead to increased skill (e.g., Ding et al., 2019, 2018; Ding and Alexander, 2023; Toride et al., 2025). We have repeated our analysis by matching on both observed SSTA and SSHA and found that forecast skill was generally lower for all variables and lead times than when matching on SSTA alone (not shown). Therefore, we limit our analog selection to observed SSTAs only.

2.3. Verification datasets

All forecasts except Taux, Tauy, and Curl are verified against the GLORYS ocean reanalysis, which includes daily and monthly mean ocean variables at 1/12° (~8 km) horizontal resolution from 1993 to 2020 (Lellouche et al., 2021). The reanalysis uses the Nucleus for European Modeling of the Ocean (NEMO) ocean model, forced at the surface by the European Center for Medium-Range Weather Forecasts (ECMWF) ERA-Interim atmospheric reanalysis. Additionally, the model assimilates along-track satellite altimetry, satellite SST, sea ice concentrations, and in situ profiles of temperature and salinity from the Coriolis Ocean database ReAnalysis (CORA) data set. Since GLORYS does not output surface wind stress fields for analysis, we verify Taux, Tauy, and Curl forecasts against the California Current System Reanalysis (CCSRA) developed at UC Santa Cruz (https://oceanmodeling.ucsc.edu/). CCSRA consists of a historical reanalysis covering 1980–2010 (Neveu et al., 2016) and an extension from 2011 to 2020. In both cases, the CCSRA employs the Regional Ocean Modeling System (ROMS) with 4-dimensional variational data assimilation (Moore et al., 2011). The domain covers nearly the entire the U.S. west coast and extends ~1000 km offshore (30–48N, 134–115.5W) with a horizontal resolution of 0.1° (~10 km) and 42 terrain-following vertical levels. Surface forcing for the 1980–2010 reanalysis is derived from a combination of ECMWF atmospheric reanalyses (ERA-40 and ERA-Interim) and cross-calibrated multiplatform (CCMP) winds, while the extension uses higher-resolution forcing from the Naval Research Laboratory's Coupled Ocean Atmosphere Mesoscale Prediction System (COAMPS). Amaya et al. (2023) showed that both GLORYS and CCSRA reasonably reproduces the observed mean state and variability of the CCS when compared to independent (i.e., unassimilated) measurements of various ocean parameters, making them useful and reliable tools for verifying our HR-MA forecasts. All GLORYS/CCSRA anomalies are relative to long-term climatology of 1994–2019 and are linearly detrended at each grid cell.

2.4. Other forecasting systems

In Section 3.4, we compare our HR-MA forecasts to a suite of dynamically downscaled forecasts produced using the same CCS configuration of ROMS as used for CCSRA (see above). Specifically, we compare the HR-MA forecasts to the ROMS forecasts generated with bias-corrected atmospheric forcing shown in Jacox et al. 2023. Due to computational constraints, the dynamically downscaled ROMS forecasts

consist of only three ensemble members initialized in January and July of each year from 1982 to 2010 (see Jacox et al. 2023 for more details). We therefore limit our comparisons between ROMS and HR-MA to a common period of 1994–2010, which is the longest overlapping period between ROMS and our verification data from the GLORYS ocean reanalysis.

In Section 3.5, we explore whether the high-resolution simulation of the coupled climate system in CESM-HR leads to overall more accurate coastal predictions in the CCS. This is done by comparing the high-resolution forecasts to a companion set of low-resolution model-analog (LR-MA) forecasts drawn from a 500-year pre-industrial control simulation that uses CESM1.3 run at a comparatively lower 1° horizontal resolution (hereafter referred to as CESM-LR). While some tuning parameters in CESM-LR were necessarily adjusted to achieve a stable top-of-atmosphere radiative balance, it is otherwise the same version of CESM1.3 as used in CESM-HR (Chang et al. 2020). We produce LR-MA forecasts using the same method as outlined in Section 2.1, limiting our data library to years 152–501 of the CESM-LR pre-industrial control to remain consistent with the size of the CESM-HR library.

To compare HR-MA and LR-MA forecasts we generate hypothetical "coastal station" data by taking GLORYS/CCSRA reanalysis data at the $0.1^\circ \times 0.1^\circ$ grid cell closest to shore at four different latitudes along the US west coast (Fig. 10m). We then use the nearest grid cells in HR-MA and LR-MA to predict each station. We use GLORYS/CCSRA for our proxy station data in order to have a consistent set of "observations" to verify all of our forecasts against and because of the limited availability of long-term *in situ* coastal ocean observations in the CCS, especially for variables other than SST and SSH. For BT forecasts, we compare HR-MA and LR-MA to GLORYS using two different representations of BT. The first simply takes the temperature at the model bottom using the grid cell nearest to the coastal station. In this case, the model bottom may be deeper or shallower than GLORYS, especially in LR-MA (Table S1). Second, we take the grid cells in CESM-HR and CESM-LR nearest to each coastal station with bottom depths deeper than GLORYS, and then vertically interpolate the 3D temperature fields at that point to the observed bottom depth (referred to as "BT-Int").

Comparisons to these proxy station data are not meant to be a quantitative assessment of how well CESM-HR and CESM-LR predict the real-world coastal environment. Instead, we use the differences between HR-MA and LR-MA forecast skill to better understand whether and how high-resolution physics improves the accuracy of the forecasts when predicting a common (and imperfect) truth.

2.5. Skill metrics

Forecast skill for each variable is estimated using the anomaly correlation coefficient (ACC) between the observed (O') and ensemble mean forecast (F') anomalies:

$$ACC(m,l) = \frac{\sum_{t=1}^{N}(F'_t(l,m)O'_t(l,m))}{\sqrt{\sum_{t=1}^{N}F'_t(l,m)^2\sum_{t=1}^{N}O'_t(l,m)^2}} \quad (3)$$

The ACC is calculated as a function of initialization month (m) and lead time (l) from 1994 to 2019 ($N = 26$) and varies from −1 to 1, with 1 being perfect and 0 being equal to chance. Note that significance is only marked for positive ACC values, which indicate potentially "useful" forecasts for decision making. To facilitate these comparisons, all GLORYS/CCSRA data were first regridded to the 0.1° CESM-HR grid. Due to the relatively slow evolution of the ocean over many months, persistence is often a good forecast for many variables in the CCS at leads of 1–6 months (e.g., Jacox et al. 2023). Therefore, analog forecasts are further compared to persistence forecasts that are generated by repeating the prior month's observed anomalies for the length of the forecast (i.e., for a January initialized forecast, using the observed anomalies from the previous December as a forecast for every lead time). Skill relative to persistence is an important measure of the added value of the forecasting system. In addition to ACC, we also assess the combined errors in the forecast mean state and variability using root mean squared error (RMSE) of the full forecast fields relative to the observations. We also quantify the bias in the parent data libraries used to generate analog forecasts (i.e., CESM-HR and CESM-LR) as well as in ROMS by differencing the mean fields between the models and GLORYS/CCSRA depending on the variable of interest. Bias and RMSE skill metrics are each standardized by the standard deviation of observed anomalies over the verification period to facilitate comparison among variables with different units.

3. Results

3.1. Evaluation of HR-MA forecasts

The HR-MA forecasts show significant forecast skill for all monthly initializations at 3-month lead for SST, SSH and BF (Fig. 3a-c). While SST forecast skill is significant throughout the domain, SSH forecasts are most skillful in a narrow coastal band from the Southern California Bight (~32N-35N) to Washington. The elevated nearshore SSH skill is likely associated with the aggregated effects of rapidly propagating coastally trapped waves, which may be associated with ENSO formation in the tropics or local wind forcing along the coast (Amaya et al., 2022). In contrast, BF forecasts are most skillful in the central and southern portion of the domain from Baja to Northern California, though there is also significant skill offshore of Oregon and Washington.

Forecasts of MLD show weak (yet significant) skill in the entire coastal zone, while forecasts of SU and SV are mostly insignificant at 3-month lead (Fig. 3d-f). Zonal wind stress forecasts have significant skill off the coast of Washington and Northern Oregon, as well as in the nearshore regions north of San Francisco Bay (~38°N) and Point Conception (~35°N) in California. Meridional wind stress forecasts are skillful primarily in the coastal regions of Northern California, with an additional region of significant skill just south of the U.S.-Mexico border. The nearshore wind stress skill corresponds with a small area of wind stress curl forecast skill near Cape Mendocino (~40°N; Fig. 3g-i), consistent with past studies showing similar forecast skill of wind driven upwelling in the central California Current System (Amaya et al., 2024). Finally, bottom temperature forecasts are skillful throughout the US west coast continental shelf (Fig. 3j-l), but especially in the coastal waters near Oregon/Washington and west of the San Francisco Bay.

Nearshore forecast skill varies substantially for different initialization months and lead times (Fig. 4). For example, SST forecasts initialized from February-April are skillful out to about 4–7 months lead, while May-August initialized forecasts are skillful out to 9–11 months lead. The elevated forecast skill for summer initialized forecasts that verify in wintertime is likely associated with deterministic ENSO teleconnections during that season. A similar pattern of elevated wintertime skill (albeit of varying magnitude) is seen in forecasts of SSH, BT, MLD, and to a lesser extent SU and SV. We will explore this topic in more detail in Section 3.3.

Forecasts of SST, SSH, BT, and MLD also have an advantage over persistence, with significant skill anywhere from 2-12 months after persistence forecasts cease to be skillful depending on initialization month (Fig. 4a-c and S1; compare white and black dots). SV forecasts initialized in summer-winter show similar improvement relative to persistence, with skill that remains significant out to ~3–4-months for July-October initializations (Fig. 4g). While nearshore forecasts of BF, Taux, Tauy, and Curl averaged over the entire US coastline are generally not skillful (Fig. 4d,h-j), the spatial maps shown in Fig. 3 suggest that there are specific regions where these forecasts may perform better. Forecasts of Taux, Tauy, and Curl do not show regional peaks in skill (not shown), however, coastal BF forecasts averaged in the Central and South CCS (see Fig. 2a for averaging domains) are noticeably more skillful than those averaged in the North CCS (Fig. 5) or across the entire

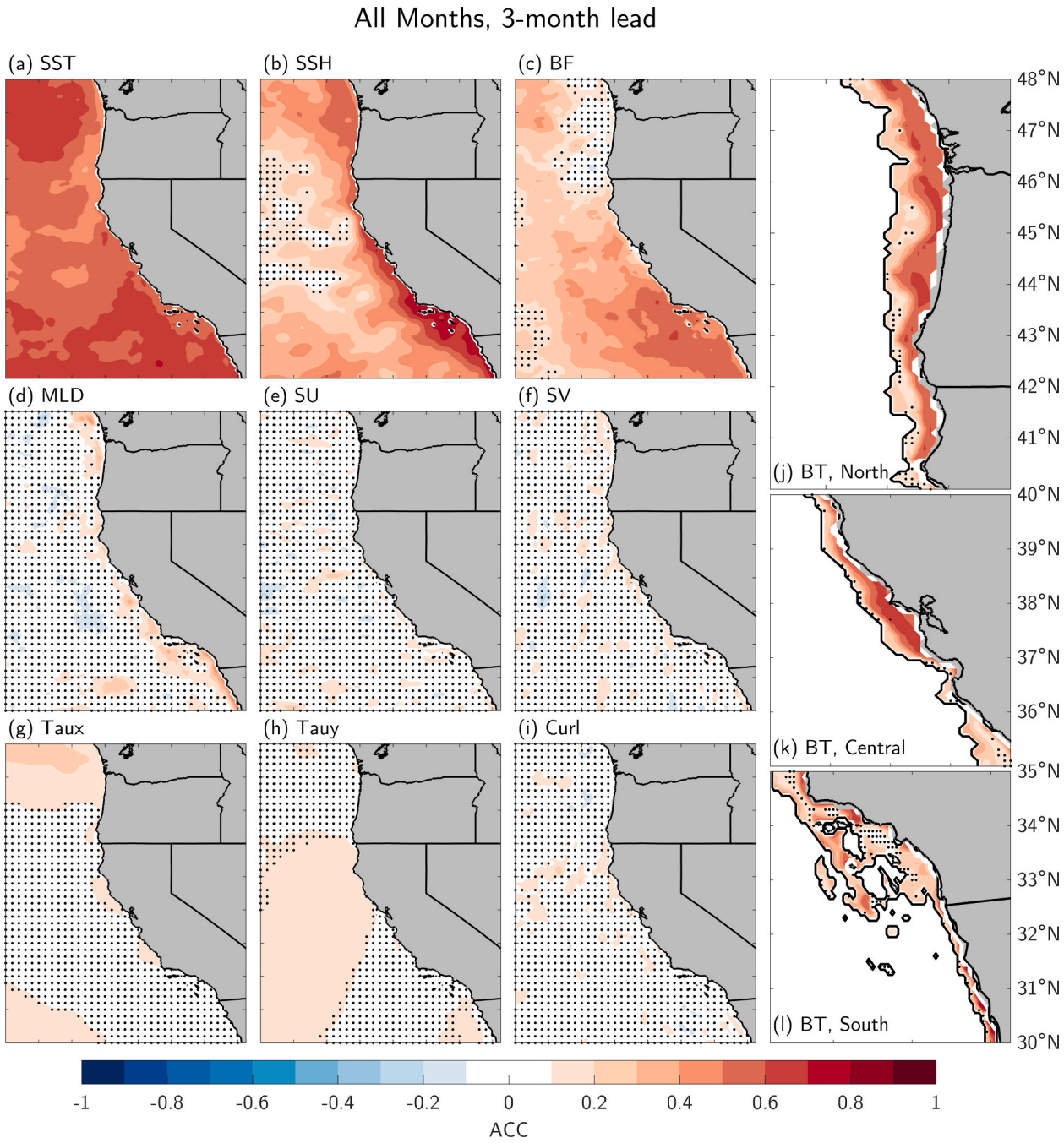

Fig. 3. (a)-(i) Ensemble mean HR-MA forecast skill at 3-month lead for all initialization months based on the top 20 matches. (j)-(l) As in (a)-(i), but for bottom temperature forecasts down to 1000 m (black contour) in three latitudinal bands. Stippling marks negative or insignificant forecast skill with 95% confidence.

CCS (Fig. 4d). Additionally, long-lead forecast skill for BF tends to peak when predicting the spring/summer (especially in the South region). This stands in contrast to a variable like SST in which the difference in forecast skill for each subregion within the CCS are relatively minor and skill peaks when predicting winter.

3.2. *Ecological forecasts*

Model-analog forecasts of the HCI have significant skill from ~1–7 months lead when initialized in December-April (Fig. 6a). There is additional skill at 3–10 months lead for HCI forecasts initialized in May-October with many of those lead times/initializations showing significant skill when persistence is not significant, once again emphasizing the likely positive impact of ENSO teleconnections on wintertime forecast skill in the CCS. Forecasts of the TOTAL tool are similarly impressive, exhibiting significant forecast skill from 6-12 months lead for nearly all potential closure months (Fig. 6b). TOTAL forecasts targeting a July (August) closure are also significant when persistence is not significant at 10–11 (12) months lead. The HR-MA HCI and TOTAL forecast skill is comparable to similar predictions made with coarse resolution initialized forecasts as well as the dynamically downscaled ROMS simulations (Brodie et al., 2023), highlighting the potential value of analog forecasting to inform marine management strategies.

3.3. *Sources of predictability*

Differences in HR-MA forecast skill across initializations and lead times arise from differences in the relative magnitude of deterministic

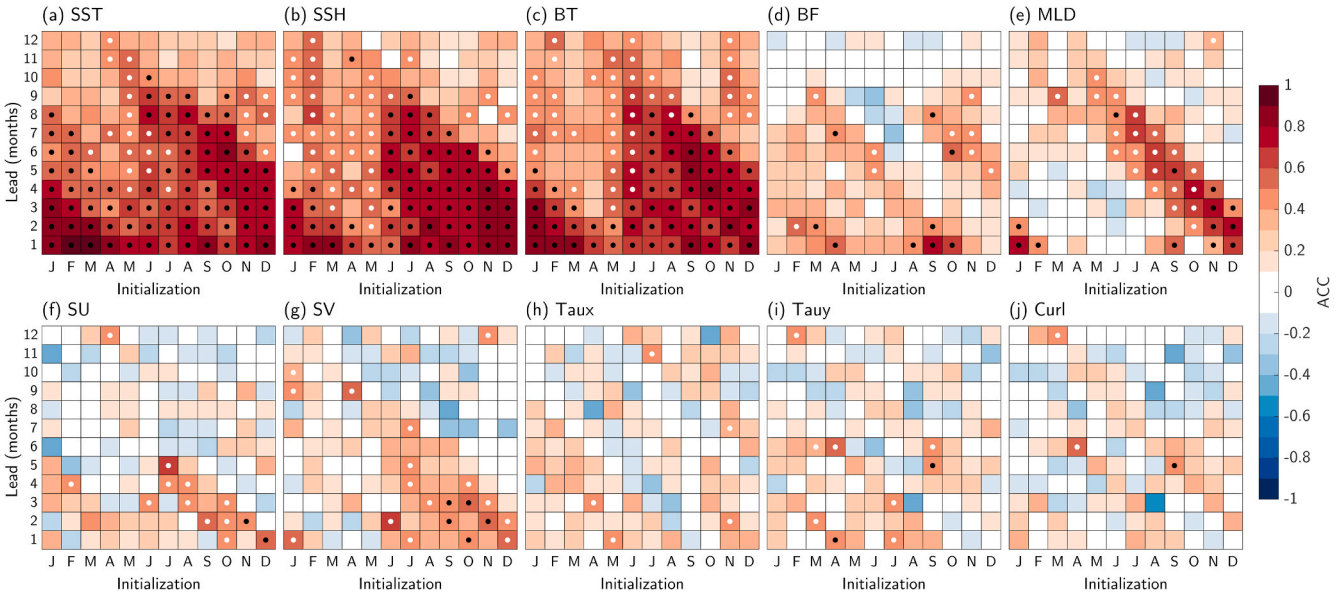

Fig. 4. Ensemble mean HR-MA forecast skill as a function of lead time (y-axis) and initialization month (x-axis), based on the top 20 matches averaged within 75 km of the coast (Fig. 2a, black contour). Black stipples mark significant HR-MA skill with 95% confidence. White stipples mark significant HR-MA skill when persistence skill is not significant.

climate signals (such as ENSO-driven wind forcing or coastally trapped waves) versus stochastic noise (such as random weather variability) as well as from the decorrelation timescale of the initial condition, which contributes to persistence. By selecting analog climate states based on specific regions that emphasize the contribution of each of these processes to skill, we attempt to isolate the primary sources of ocean predictability in the CCS and gauge to what extent the analog selection method is capturing the relevant physics.

When selecting analogs based on CCS SSTAs only (i.e., orange shading in Fig. 1), January initialized HR-MA forecasts have similar skill patterns to the corresponding persistence forecasts (Fig. 7a-b). For example, the HR-MA SSTA skill is generally highest at the earliest lead times before weakening over the length of the forecast, consistent with the SSTA persistent forecast skill. Similar characteristics are found for July (Fig. 7e-f) and the other monthly initializations (Fig. S2a). Overall, the differences between persistence and the HR-MA SSTA forecasts in this CCS-only configuration are small, with $\Delta ACC < +/- 0.2$ for 1–11 months lead (Fig. S2a). The close correspondence between the SSTA analog and persistence forecasts makes sense as SSTA differences are the basis for analog selection. As a result, we are more likely to identify model climate states that are close to the observed initial SSTA state within the CCS, while deemphasizing other possible sources of predictability outside of the forecast domain. Ultimately, this leads to SSTA forecasts whose subsequent skill primarily derives from the month-to-month persistence of that initial state.

For other variables that have initial states that are reliably linked to the CCS SST initial state, the corresponding model field is also likely to be close to its observed initial state, leading to skillful persistence-based predictions at early lead times. For example, CCS-only SSH forecasts compare well to persistence, particularly for July initializations (Fig. 7a-b, e-f). However, because SSHA was not used for choosing analogs, the match to the observed initial SSH state is not as close as it is for SST, leading to overall less skillful SSH forecasts in the first 1–6 months of the forecast depending on initialization month (Fig. S2b). The impact of a less accurate initial state is further highlighted by subsurface variables that are not always strongly linked to the SST initial state, like BT. For example, CCS-only BT forecasts initialized in July-October are noticeably less skillful than persistence from 1-12 months lead, depending on month, with ΔACC as large as -0.52 (Fig. 7e-f and S2c, seventh column). In contrast, BT forecasts initialized in November-April are closer to persistence from 1-7 months lead ($\Delta ACC = +/- \sim 0.2$). In summertime, the upper ocean is highly stratified and ocean mixed layers are shallow, leading to bottom waters that are mostly insulated from the physical characteristics of the surface (e.g., Alexander et al., 2023). Therefore, we would not necessarily expect the SSTA initial state to be a good indicator of the BT initial state in summer. In winter, however, the characteristics of surface and bottom waters are linked by deepened mixed layers, making it more likely that analogs chosen based on SST differences would have an accurate initial BT state. Still, the accuracy of a given variable's initial state and, by extension, the skill of the subsequent persistence forecast could likely be optimized by selecting analogs based on the respective variable's differences (i.e., if BT is the target variable, selecting analogs based on BT differences instead of SSTA differences). Overall, however, these results highlight persistence as an important source of seasonal predictability in the CCS (and likely in other regions), particularly within the first few months of a forecast.

When instead selecting analogs based on tropical SSTAs only, forecast skill for most variables peaks when predicting winter-spring conditions (Fig. 7c,g). For example, January initialized analog forecasts have the highest skill between 1–5 months lead (i.e., verification months January-April), while July initialized forecast skill peaks at 5–8 months lead (i.e., verification months November-February) depending on the variable (Fig. 7c,g). January and other wintertime initialized forecasts have peak skill that is similar to persistence at early leads for most variables, however, the July initialized peak skill is noticeably better than persistence for SST, SSH, BT, MLD, and SV (Fig. S3), suggesting that these forecasts benefit from an additional source of predictability. Selecting model climate states based on tropical SSTAs ensures that tropical climate modes in the analog forecast initial state have a similar phase and intensity as in observations. The subsequent progression of a given analog forecast is likely then partially dictated by the simulated evolution of these tropical modes and their teleconnections to the CCS, plus whatever local stochastic variability is inherent to that climate state. Averaged over the top matches, much of the random variability unique to each analog cancels out, while the deterministic climate signal common to all the ensemble members remains to positively contribute to forecast skill during boreal winter and spring. These results further point to tropical teleconnections as an important source of deterministic forecast skill in our analog forecasts, consistent with previous studies using other forecast systems (e.g., Amaya et al., 2022; Jacox et al., 2018;

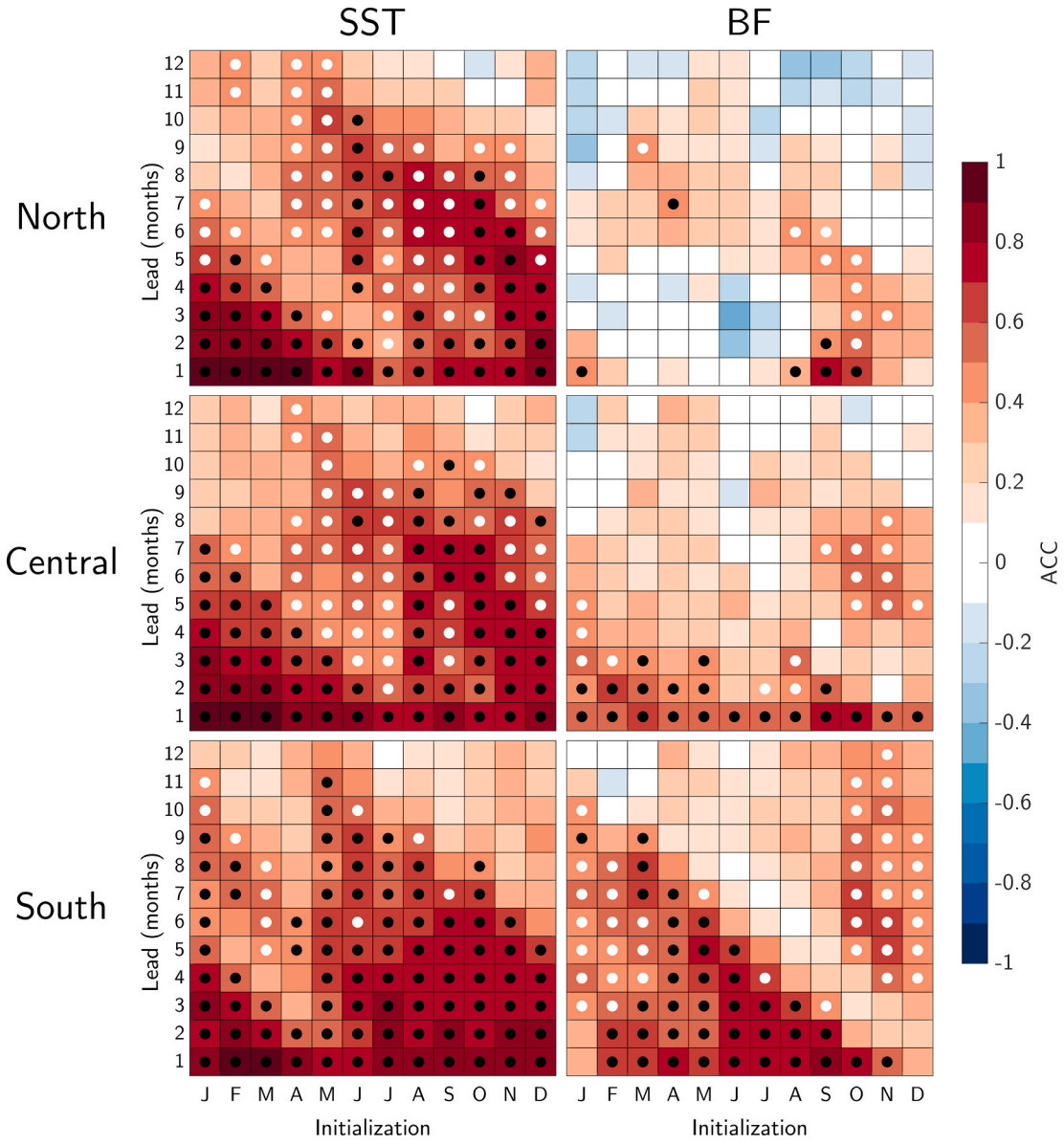

Fig. 5. As in Fig. 4, but for HR-MA SST (left column) and BF (right column) forecasts averaged within coastal subregions (Fig. 2a, dashed lines).

Xu et al., 2024).

Analog forecasts based on equally weighted SSTA differences in the tropics and CCS (i.e., as in Figs. 3-6) have skill patterns that largely reflect the combined contributions of persistence and tropical teleconnections to predictability across lead times (Fig. 7d,h). For example, January initialized SST forecasts are significant from 1-8 months lead, consistent with persistence. July initialized forecasts of SST, SSH, MLD, SU, and SV show improvements to persistence-based skill at 1–9 months lead, depending on the variable (Fig. 7h and S1). The lead times and initialization months of the largest skill over persistence for each variable correspond well with those seen when matching on tropical SSTA alone (comparing Figs. S1 and S3), suggesting that the additional skill for these lead times is likely the result of tropical teleconnections associated with the analog's more accurate tropical initial state. However, despite largely capturing the combined contribution of persistence and tropical teleconnections to overall forecast skill, some forecasts in the tropics + CCS analog configuration are less skillful than if tropical SSTAs alone were used as the selection criteria. For example, tropics + CCS forecasts of SSH, BT, and SV are all noticeably worse than the corresponding tropics-only forecasts when forecasting winter and spring at leads greater than ~6 months (comparing Figs. S1 and S3). This suggests that the additional emphasis on the CCS during the analog selection process may degrade the quality of the tropical initial state in the analog forecasts and potentially negatively impact skill derived from teleconnections. Still, tropics + CCS forecasts of SST, SSH, and BT at short lead times (< ~3 months) are generally more skillful than those based on the tropics-only (comparing Figs. S1 and S3), indicating that the additional emphasis on the CCS may actually improve the prediction skill of some variables early in the forecast. Overall, these results make it clear that the analog selection method should be tailored to emphasize the predictability of particular variables or target seasons. We will discuss this concept in more detail in Section 4.

Finally, it is interesting that the January initialized CCS-only forecasts of SST, SSH, and BT show elevated skill beyond ~8-months relative to the tropics-only forecasts (comparing Fig. 7b-c). This may suggest that there are other local dynamics captured by a more accurate CCS initial state that positively contribute to long-lead skill for January initializations. However, by considering all initialization months (Figs. S2-S3), we see that long-lead CCS-only SSH and BT forecasts are not noticeably better than the tropics beyond the January initialization, implying that

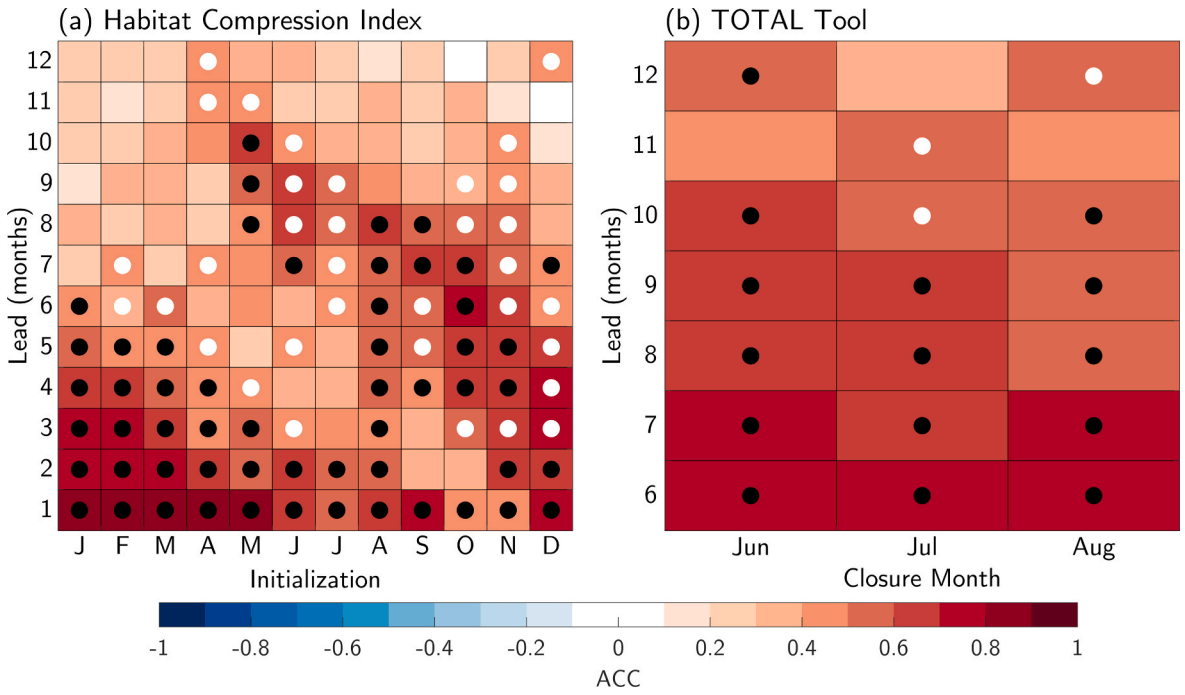

Fig. 6. Ensemble mean HR-MA forecast skill of (a) HCI and (b) TOTAL tool as a function of lead time (y-axis) and initialization month (x-axis), based on the top 20 matches. Stipples are as in Fig. 4.

the difference is likely an artifact associated with the relative signal-to-noise characteristics of the two forecast systems. Still, the CCS-only SSH, BT, MLD forecasts do show elevated skill relative to persistence at long-leads in a similar pattern as seen in the tropics-only and tropics + CCS model-analog configurations (Fig. S2). Local dynamics emphasized by the CCS-only framework (e.g., reemergence) could play a role in driving this added predictability. However, it is more likely that this elevated skill is the result of aliasing tropical forcing during the analog selection process.

In particular, while ENSO forcing of the CCS takes ~1–2 months (e.g., Alexander et al., 2002; Jacox et al., 2015), the persistence of these anomalies can last beyond the initial forcing, leading to high simultaneous correlations between ENSO and oceanic variables within the CCS. As a result, even when selecting 20 analogs based on SSTAs in the CCS alone, it is likely that a fraction of these analogs will also feature a tropical initial state similar to observations. Indeed, the CCS-only analogs do a reasonable job of reconstructing the observed Nino3.4 index at each initialization (R = 0.63; Fig. S4b), despite not using any tropical information as part of the analog selection criteria. In general, we find that the CCS-only configuration shares between 2–3 of its top 20 analogs with the tropics-only configuration on average, with that number rising to as many as 11 during the 1997–1998 El Niño (not shown). Even if we control for common analogs, instead selecting the top 20 CCS-only analogs at each time step that are not also present in the top 20 of the tropics-only, we still find that these "independent" CCS-only analogs reasonably capture the observed tropical initial state at each time step (R = 0.47, Fig. S4c). Therefore, while the CCS-only forecasts certainly emphasize persistence forecast skill at early leads times, this method is clearly an imperfect measure of the effects of local dynamics on forecast skill.

3.4. Comparisons to dynamically downscaled ROMS

We now compare HR-MA forecasts to those from a dynamically downscaled ROMS simulation (Jacox et al. 2023), which allows us to qualitatively assess HR-MA forecasts relative to a more computationally demanding alternative. January initialized ROMS forecasts have significant SST skill at 3-month lead for much of the nearshore CCS (within ~75 km), with skill increasing from central California to the northern-most coastal waters of Washington and then offshore (Fig. 8a). The elevated coastal SST skill is primarily due to strong persistence at 1–4 months lead (Fig. 9a), likely resulting from relatively deep winter-time MLDs which increase thermal inertia and help to propagate the initial condition from month-to-month.

To compare apples-to-apples, we first compare ROMS to January initialized HR-MA forecasts based on the top 3 analog matches (Fig. 8b and 9b). Overall, the 3-member HR-MA and ROMS simulations show similar forecast skill patterns, with generally small quantitative differences in either direction that are dependent on region (Fig. 8d), lead time, and initialization month (9a-b, d-e). The coastal averaged SST forecast skill for the 3-member HR-MA is also very similar to ROMS, with significant skill out to 5-month lead that is also primarily attributable to persistence (Fig. 9b). These similarities mostly extend to other variables and lead times, with ROMS and the 3-member HR-MA forecasts displaying comparable skill patterns in terms of magnitude and/or significance for SSH, BT, MLD, SU, SV, Taux, Tauy, and Curl. One exception is BF forecasts, where ROMS has significant nearshore skill relative to persistence at 5–7 months lead, while the 3-member HR-MA does not. Expanding the HR-MA ensemble size to the top 20 matches markedly increases January initialized SST forecast skill at 3-month lead (Fig. 8c). Here, the 20-member HR-MA forecasts are generally more skillful than the 3-member ROMS nearly everywhere in the domain. The additional HR-MA ensemble members also noticeably improve the skill of some nearshore averaged variables such as SST, SSH, and BT (Fig. 9c).

The added value of a larger HR-MA ensemble size is more clearly illustrated by July initialized forecasts (Fig. 9d-f and S5). For example, ROMS forecast skill above persistence peaks at ~6–10 months lead for SST, SSH, and BT (Fig. 9d). While the 3-member July initialized HR-MA forecasts are notably less skillful than ROMS across nearly all lead times and variables, they display similar seasonal characteristics with elevated skill at lead times verifying in winter and spring for SST, SSH, and BT (Fig. 9e). In comparison, the 20-member HR-MA forecasts more clearly reproduce and even improve upon the July initialized skill seen in the ROMS simulations (Fig. 9f). For example, 20-member HR-MA SST, SSH,

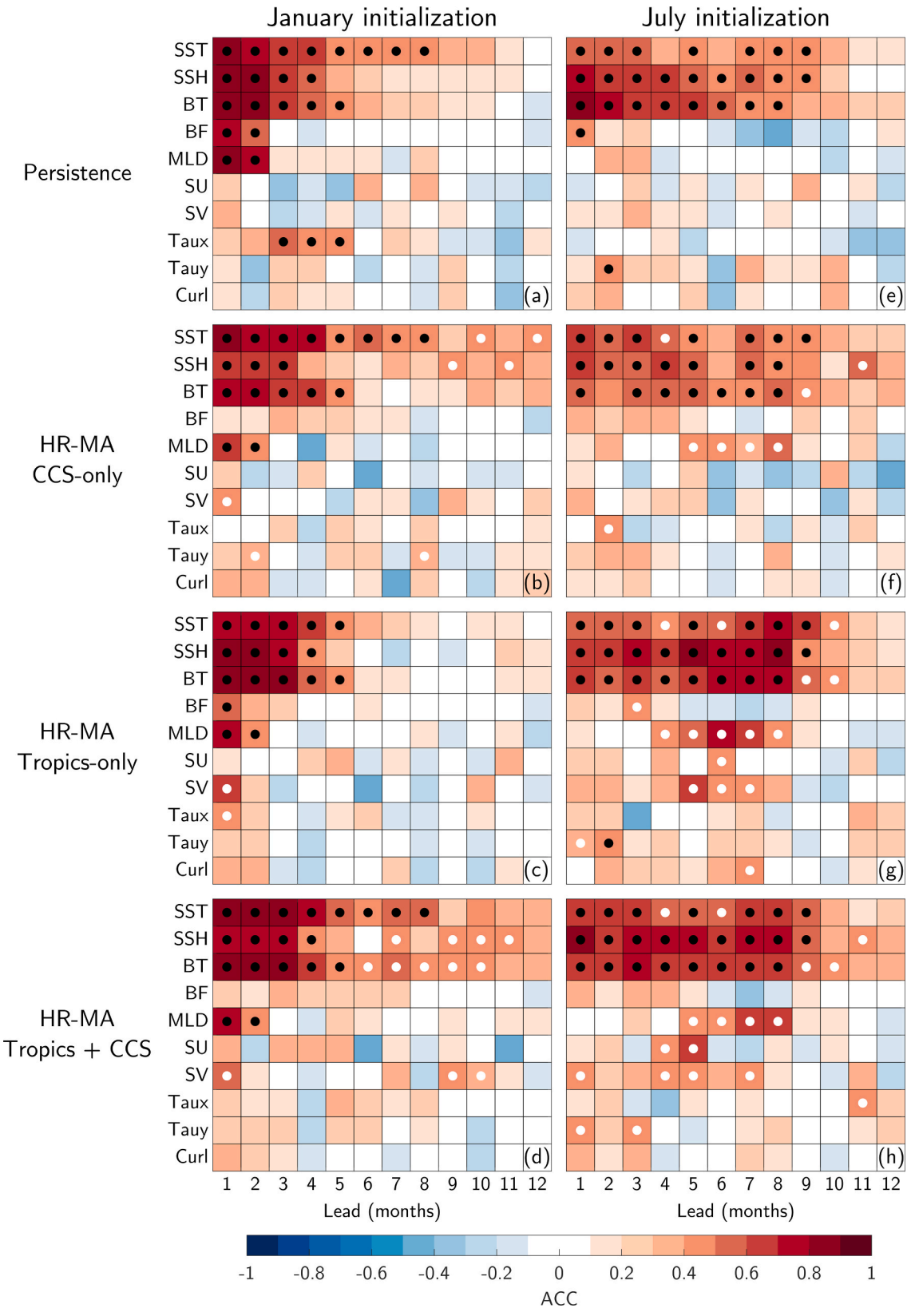

Fig. 7. (a) Skill of January initialized persistence forecasts averaged within 75 km of the coast (Fig. 2a, black contour). (b) As in (a), but for HR-MA forecasts selected using SSTA differences in the CCS alone (Fig. 1, orange shading). (c) As in (a), but for HR-MA forecasts selected using SSTA differences in the tropics alone (Fig. 1, green shading). (d) As in (a), but for HR-MA forecasts selected using SSTA differences in both the tropics and CCS, equally weighted (i.e., Eq. (1)). (e)-(h) As in (a)-(d), but for July initialized forecasts. All HR-MA forecasts are based on the ensemble mean of the top 20 matches for each respective analog selection criteria. Stipples are as in Fig. 4.

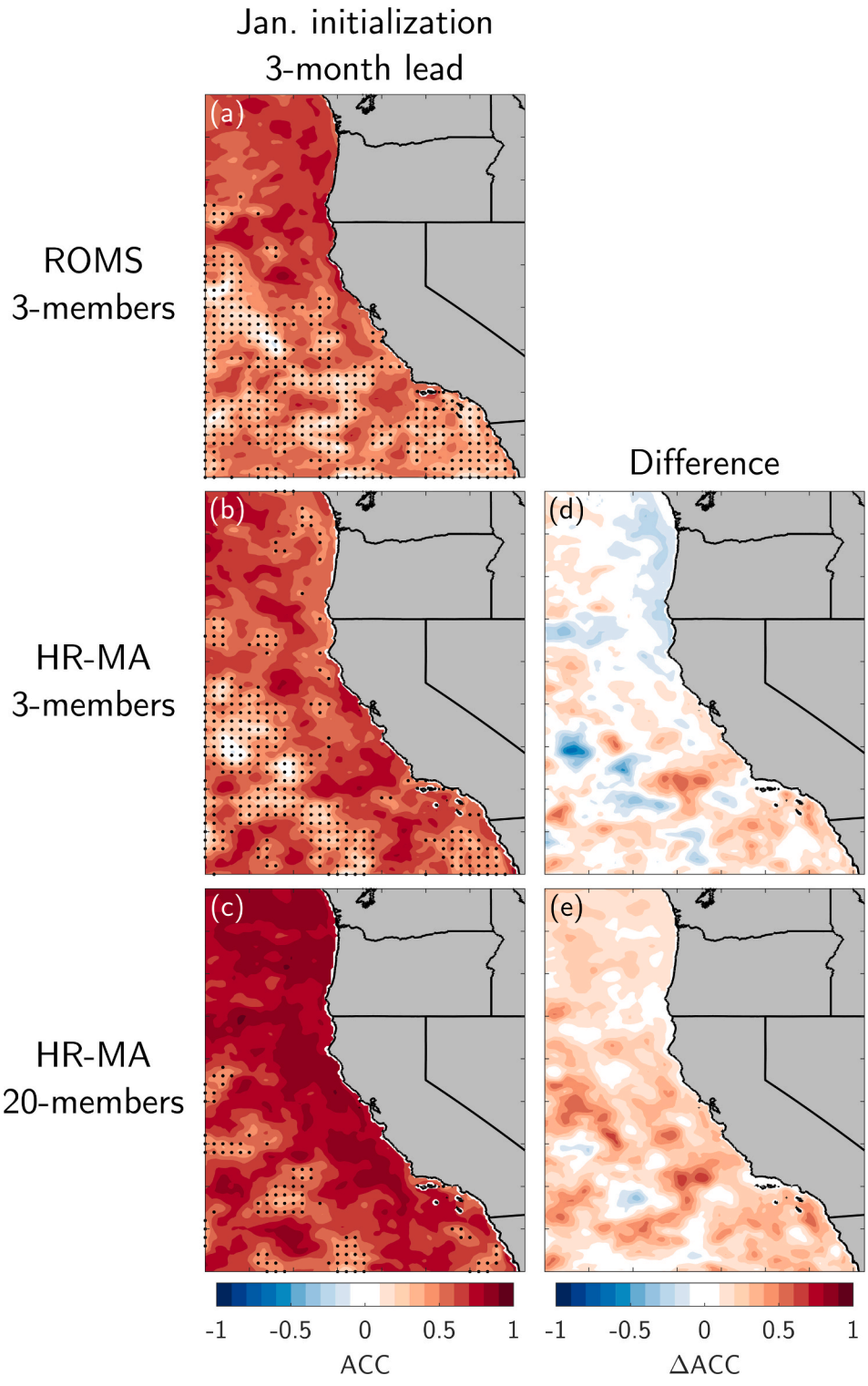

Fig. 8. (a) Ensemble mean skill of January initialized SSTA forecasts at 3-month lead from the 3-member dynamically downscaled ROMS (Jacox et al. 2023). (b) As in (a), but for the top 3 HR-MA matches. (c) As in (a), but for the top 20 HR-MA matches. (d) Difference of (b) minus (a). (e) Difference of (c) minus (a). Stippling in (a)-(c) mark negative or insignificance forecast skill with 95% confidence.

and BT forecasts are mostly comparable to those from ROMS, with significant skill at early leads of 1–5 months and elevated skill relative to persistence at leads exceeding 6-months (especially for BT). However, the 20-member HR-MA ensemble has noticeably higher skill for MLD forecasts at 5–8 months lead. Given the lack of similar MLD skill in the 3-member HR-MA, it is likely that the enhanced skill in the 20-member ensemble is due to a more robust representation of ENSO-related teleconnections via a higher forecast signal-to-noise ratio.

In terms of RMSE, both ROMS and HR-MA show similar skill for most variables and lead times with a few notable exceptions (Fig. S6). Both the 3-member and 20-member HR-MA have a lower RMSE for BF at all lead times regardless of initialization month, while ROMS has a lower RMSE for MLD when forecasting boreal summer and fall and for Curl when forecasting spring and early summer (Fig. S6). The differences in

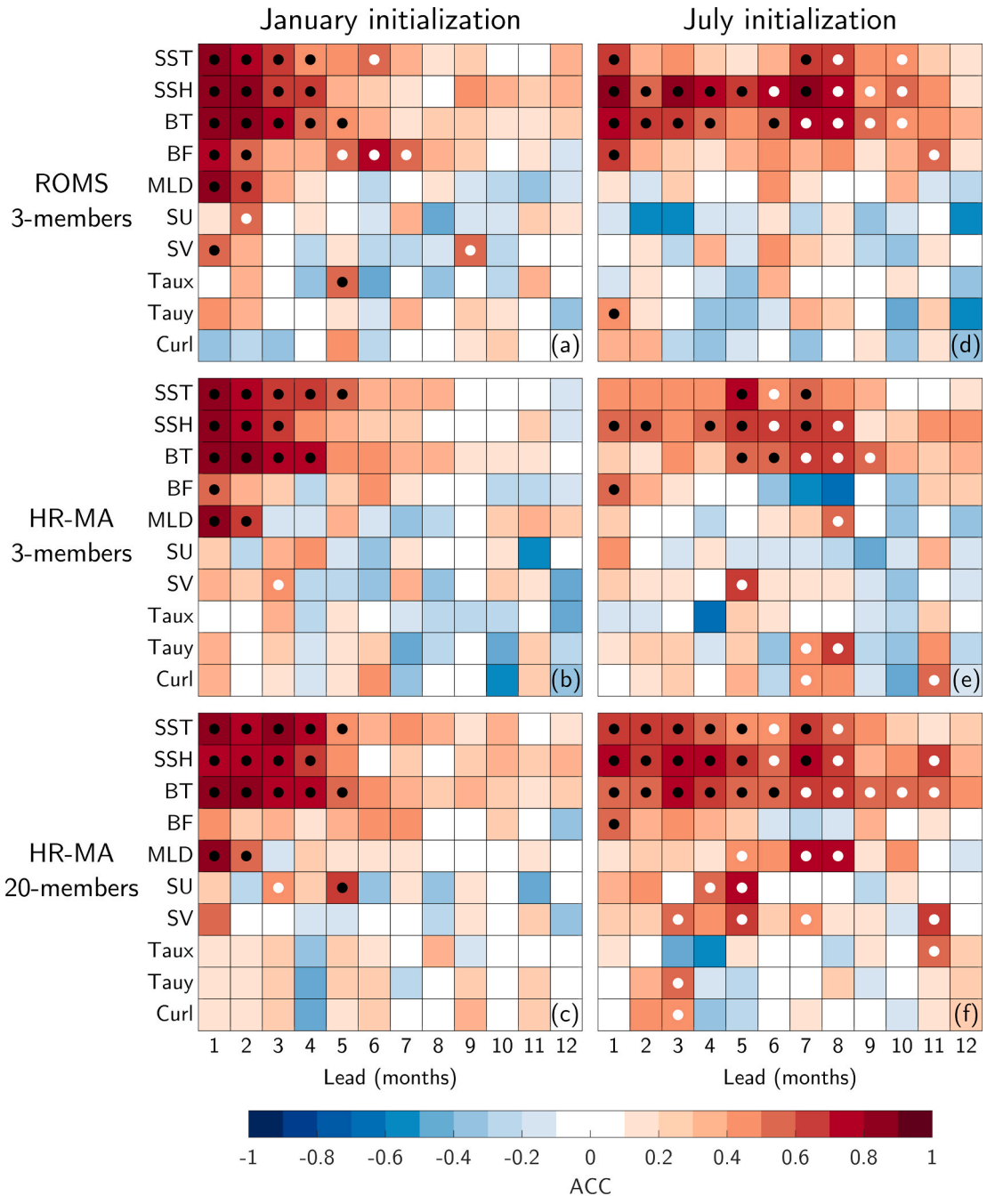

Fig. 9. (a) Ensemble mean skill based on ACC of January initialized forecasts from the 3-member dynamically downscaled ROMS averaged within 75 km of the coast (Fig. 2a, black contour). (b) As in (a), but for the top 3 HR-MA matches. (c) As in (a), but for the top 20 HR-MA matches. (d)-(f) As in (a)-(c), but for July initialized forecasts. Stipples as in Fig. 4.

RMSE between HR-MA and ROMS are primarily driven by differences in their respective mean biases (Fig. S7). Note that ROMS was forced with bias-corrected atmospheric model output, resulting in generally smaller biases in the ocean forecasts (Jacox et al., 2023).

We emphasize that the comparisons between HR-MA forecasts and those from ROMS are necessarily qualitative, and are not meant to indicate that one method is demonstrably "better" than the other. There are many factors that could explain the differences between the skill patterns described here, including the underlying forecast model, the initialization data and method, and/or the ensemble size. For example, it is likely that the dynamically downscaled ROMS forecasts would see a similar improvement in skill if also expanded to a 20-member ensemble (Jacox et al., 2020). Indeed, the ROMS forecasts could, in theory, consist of an infinitely large ensemble of uniquely initialized members. In contrast, the quality of the model-analog members degrades as the ensemble size grows. Although, expanding the ROMS ensemble incurs a much higher computational cost than expanding the model-analog ensemble. Overall, our ability to largely reproduce (and in some cases exceed) the skill of a relatively expensive regional model forecast, while also having the capability to analyze additional initializations beyond just January and July and additional regions beyond the CCS, directly underscores the added value of the model-analog method.

3.5. *High-resolution vs low-resolution analog forecasts*

Finally, we explore the added value of increased model resolution to

forecasts of the nearshore environment in the CCS. When calculated for all initialization months, the skill (as measured by ACC) of the LR-MA "coastal station" forecasts is strikingly similar to the corresponding HR-MA forecasts (Fig. 10), with ΔACC < +/- 0.1 for most variables and lead times. This is consistent with Little et al. (2024) who showed that sea level variability in identically forced versions of high-resolution (0.1°) and low-resolution (1°) CESM1.3 is strongly correlated along the US west coast, though the high-resolution simulation had more overall sea level variance. The most noticeable and consistent improvements are for HR-MA BT forecasts at 40°N and 30°N, where the ocean depth of the nearest CESM-LR grid cell is too deep to reliably capture the variability of temperature at the observed bottom depth of those coastal stations (Table S1). This problem can largely be alleviated by vertically interpolating the LR water column temperature to the true bottom depth (BT-int cf. BT), though this non-trivial post-processing step may hinder uptake of global model output for bottom temperature. Additionally, HR-MA shows notable improvements in SU forecasts at 40°N, with ΔACC peaking at 0.32. The benefits of high-resolution are more evident when considering standardized RMSE across the different variables and lead times (Fig. 11). In particular, the largest improvements in RMSE are in HR-MA forecasts of SST, SSH, MLD, and, to a lesser extent, BT-Int. In contrast, LR-MA forecasts have a lower RMSE for Curl at 30°N. The improvements in SST, SSH, and MLD RMSE are at least partially due to smaller nearshore mean state biases in CESM-HR versus CESM-LR (Fig. S9). Large BT biases in LR-MA are primarily due to the deeper ocean bottom, though they are substantially reduced when interpolating CESM-LR temperature data to the observed bottom depth (i.e., BT-Int). Overall, the HR-MA forecasts are generally more accurate in an absolute sense. However, both the HR-MA and LR-MA forecasts similarly capture the observed timing of nearshore CCS variability, suggesting that even relatively coarse (~1°) resolution models could provide useful management support tools, consistent with Brodie et al. (2023).

4. Summary and Discussion

In this study, we used the model-analog forecasting technique to generate a suite of computationally efficient high-resolution (0.1°) seasonal ocean forecasts of the CCS based on CESM-HR. Forecasts of SST, SSH, BT, BF, and MLD were the most accurate, with significant skill at 6–12 months lead when forecasting boreal winter, depending on the variable (Figs. 3-5). Forecasts of ecological indices such as the HCI and TOTAL tool were also skillful at up to 12-months lead, depending on initialization month (Fig. 6). By selecting analogs based on different regional SSTA differences (i.e., the CCS-only, the tropics-only, and CCS + tropics), we explored different sources of predictability within the CCS, as well as their relative contribution to the overall HR-MA forecast skill (Fig. 7). We showed that enhanced skill seen in many variables during winter primarily resulted from deterministic climate forcing associated with tropical teleconnections. However, persistence was also found to be a major source of predictability, particularly at early lead times. We further showed that the HR-MA forecasts are comparably skillful to more expensive alternatives generated by dynamically downscaled regional ocean models (Figs. 8-9). When incorporating a larger ensemble size, the HR-MA mostly exceeded the skill of the

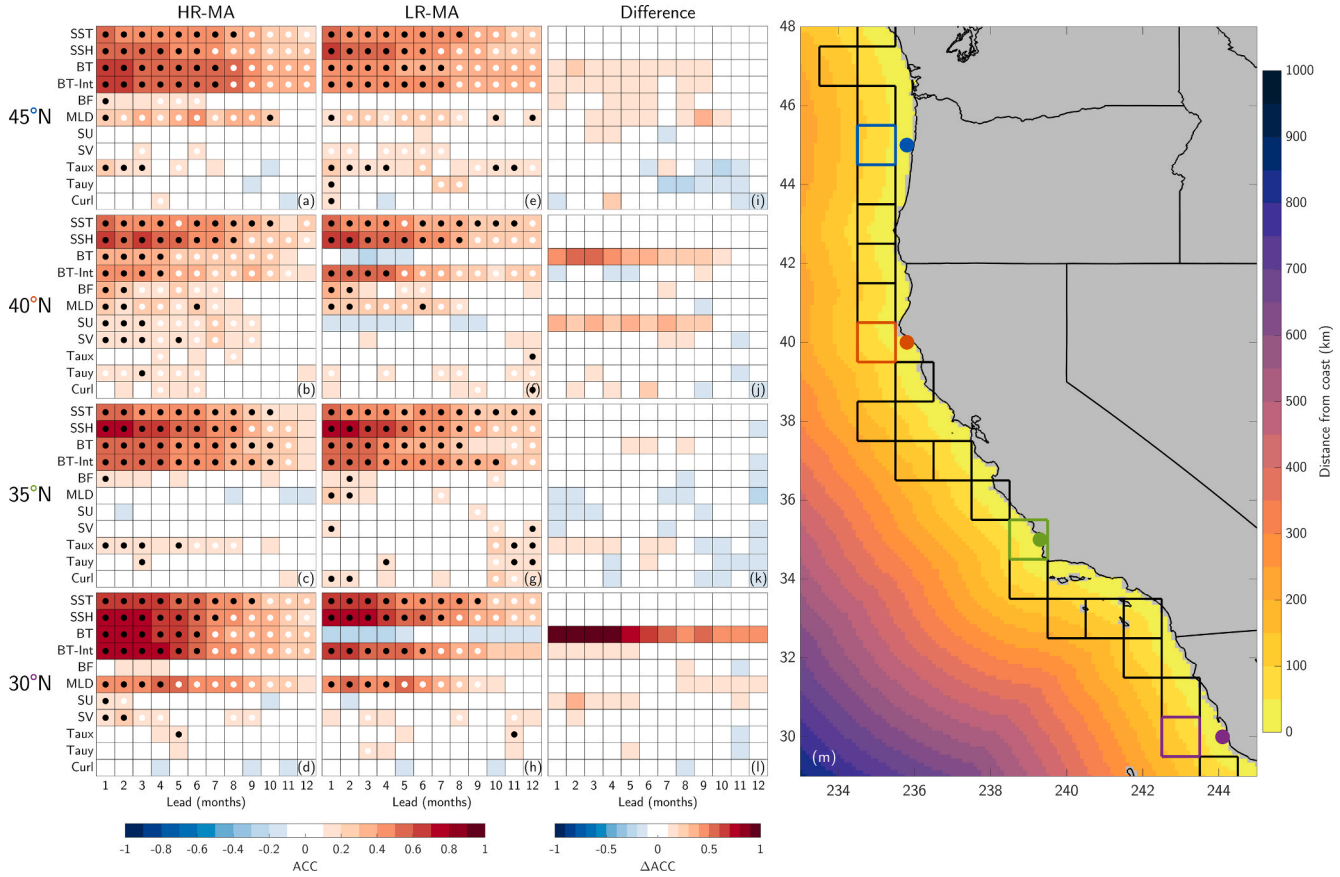

Fig. 10. (a)-(d) Ensemble mean HR-MA forecast skill at four "coastal stations" (see Section 2.4 for details) for all initialization months. (e)-(h) As in (a)-(d), but for ensemble mean LR-MA forecasts at the closest grid cells to each "coastal station". (i)-(l) The difference of HR-MA minus LR-MA forecasts at each "coastal station". Both the HR-MA and LR-MA forecasts are based on the average of the top 20 matches. (m) Location of each "coastal station" used for HR-MA forecasts and the GLORYS/CCSRA verification data (colored dots). Black boxes denote the 1° × 1° CESM-LR SST grid cells closest to land. Colored boxes mark the CESM-LR SST grid cells closest to the "coastal station" of the same color. The closest grid cells for other CESM-LR variables are shown in Fig. S8. Shading is the distance of each 0.1° ocean grid cell in CESM-HR from the nearest land grid cell. Stipples are as in Fig. 4.

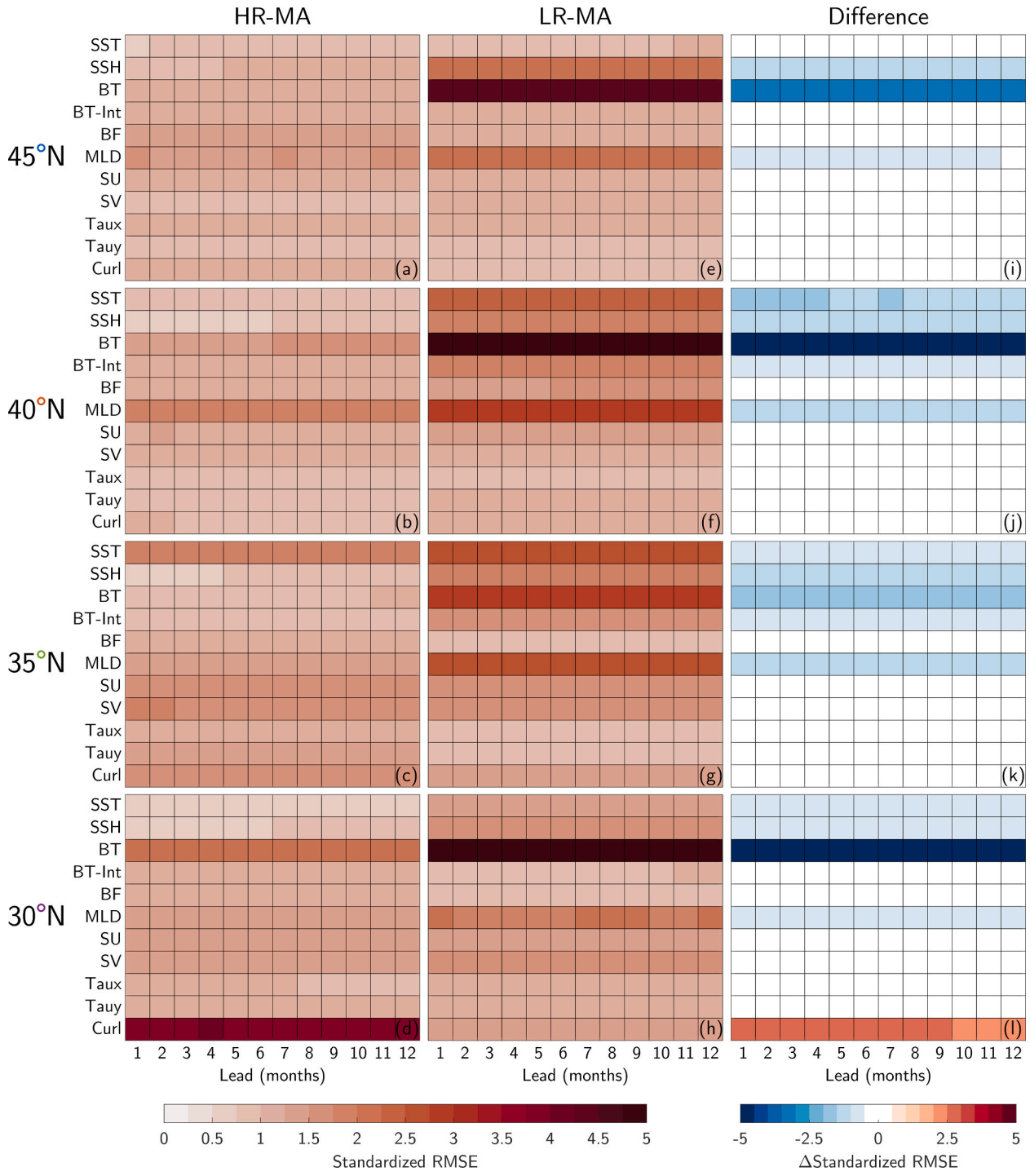

Fig. 11. As in Fig. 10a-l, but for the standardized RMSE at each "coastal station".

regional model forecasts, which only had 3 members. Finally, we showed that comparatively low-resolution (1°) analog forecasts of the CCS coastal environment have similar ACC skill as their high-resolution counterparts, though the HR-MA forecasts were generally more skillful in an absolute sense due largely to reduced biases (Figs. 10-11).

Our results have several important implications for marine resource management in the CCS, for research into the model-analog technique, and for high-resolution seasonal climate forecasting as a whole. First, we echo several recent studies (Amaya et al., 2024, 2022; Brodie et al., 2023; Jacox et al., 2023, 2020; Tommasi et al., 2017) highlighting global climate models as potentially valuable inputs to decision support tools for marine resource management. The ability of models like CESM-HR and CESM-LR to accurately represent the observed evolution of the nearshore CCS is impressive, especially given that these simulations were not necessarily optimized to capture the coastal environment. Still, while we and others (e.g., Jacox et al. 2023) demonstrate significant high-resolution forecast skill for many ocean parameters in the CCS, it is important to continue to work with marine resource managers in the region to clearly identify how such forecasts can tangibly inform the decision-making process.

Second, our investigation into sources of predictability in the CCS (Fig. 7) makes plain the sensitivity of model-analog forecasting to the

selection criteria used to identify analog climate states, including the matching domain and the specific variable differences being examined. There simply is not a single analog selection criterion that will maximize the forecast skill of every variable at every lead time. However, it is clear that the model-analog approach is most useful when forecasting regions/variables that are strongly influenced by tropical teleconnections (e.g., ENSO). The analog selection method can then be further optimized to capture other key sources of predictability of a specific parameter of interest (i.e., persistence), with the possible side effect of simultaneously weakening the forecast skill of other variables. Machine learning techniques have recently been leveraged to fully optimize the weighting function used to select analogs (either in space or in the number and type of parameters used to identify climate states) in order to maximize the forecast skill of specific variables or lead times (e.g., Rader and Barnes, 2023; Toride et al., 2025). Similar methods could be employed in the future to improve forecast skill of high-resolution ocean conditions relevant for marine resource management, whether that be for certain variables (such as SSH for coastal inundation) or target seasons (such as summer for the TOTAL tool). Additionally, while our study successfully draws skillful forecasts from a pre-industrial control run, it is possible that such simulations will yield increasingly poor analog climate states as anthropogenic climate change continues to unfold, especially in regions where the stationarity of internal variability cannot be assumed (e.g., Alexander et al., 2018). Various methods have been proposed to account for climate change in analog forecasting, ranging from adding an estimate of external forcing to model-analog forecasts derived from pre-industrial control runs (e.g., Ding et al. 2019) to drawing analogs from large ensemble climate simulations with time-varying radiative forcing (e.g., Ding and Alexander, 2023; Lou et al., 2025). In terms of variability, the pre-industrial climate still appears to be a reasonable proxy for recent observations in the CCS, as evidenced by the skill of our HR-MA forecasts. However, future applications of the model-analog method should carefully consider the magnitude of externally forced trends relative to local internal variability when deciding the type of data library to incorporate.

Third, given that the LR-MA forecasts were in many ways just as skillful as the HR-MA forecasts, it is reasonable to wonder what value high-resolution physics adds to seasonal forecasts of the CCS? After all, if an end-user is primarily interested in predicting the timing of above or below average ocean conditions, then the 1° model may be just as useful a tool as the 0.1° model. On the one hand, the similarity between the LR-MA and HR-MA forecasts is not surprising. Seasonal-interannual variability in the CCS is dominated by large-scale forcing from tropical teleconnections, with the entire US west coast often experiencing a same sign seasonal anomaly in response to ENSO-driven wind changes. Since ENSO is a major source of seasonal predictability in the CCS, it then makes sense that forecasts of ocean conditions within ~100 km of the coast would be similarly skillful as forecasts within ~10 km. Indeed, when we repeat our analysis by selecting HR analogs based on SST data on a 1° grid, our results and conclusions remain qualitatively unchanged (not shown). This suggests that even a coarsened representation of ENSO and the initial ocean state is adequate to capture the most predictable components of the CCS, even at higher resolutions. It is also possible that the similarities between the HR-MA and LR-MA forecasts are due to the analog selection process itself. For example, by selecting analogs based on tropical SSTA differences, we emphasized an important source of both basin-scale and mesoscale seasonal ocean predictability, namely ENSO.

On the other hand, there are mesoscale processes that are likely captured in CESM-HR that we might have expected to either provide additional sources of predictability on small scales or otherwise "scale-up" and improve the representation of large-scale variability in the model. For example, coastally trapped waves are an importance source of coastal SST, SSH, and BT predictability in the CCS (Alexander et al., 2025; Amaya et al., 2022), and with spatial extents of ~20–50 km in the CCS, these relatively narrow features may not be explicitly resolved in CESM-LR. Although, some studies have shown that coarse resolution models can have coastally trapped waves of lower amplitude than observed (Small et al., 2024). If we had tailored our analog selection method (perhaps via machine learning) to better capture the initial state of some of these mesoscale features, then it is possible that the HR-MA forecasts would show additional gains over the LR-MA forecasts. Still, this assumes that the evolution of these mesoscale features is predictable on seasonal timescales, which may not always be the case. Instead, it could be that high-resolution physics improves ocean predictions primarily on subseasonal-to-seasonal timescales (Weeks 1–6). Even on seasonal timescales, though, we did see improvement in the mean biases of the HR-MA (Fig. S9), which is consistent with Chang et al. (2023) and presumably results from a better representation of the mesoscale physics and coastal bathymetry in the model. Since many ecological models ingest total fields of oceanographic variables (e.g., SST rather than SSTA), significant mean state biases can degrade their predictions, necessitating additional processing to correct for those biases prior to analysis (Jacox et al., 2023). Therefore, a more accurate mean state in the HR-MA forecast is a welcome improvement. Overall, our results echo Brodie et al. (2023) and suggest that low-resolution models could be a reliable tool to support marine management decisions in the CCS on seasonal timescales. However, we encourage additional research to further untangle the added benefits of high-resolution modeling to ocean forecasts in this and other regions.

Finally, our findings build on a growing body of literature (Ding et al., 2019, 2018; Lou et al., 2025, 2023; Menary et al., 2021; Rader and Barnes, 2023; Toride et al., 2025) highlighting the model-analog forecasting technique as a computationally efficient alternative to traditional initialized forecasting. In particular, we have shown that model-analog forecasts drawn from an existing high-resolution climate model could successfully overcome many of the computational bottlenecks associated with operational seasonal ocean forecasting. In the future, the analog method could be further leveraged to explore the predictability of other difficult to simulate systems. For example, increasing the availability of ocean biogeochemical (BGC) forecasts would broaden the potential ecological applications of high-resolution ocean predictions (e.g., Siedlecki et al., 2016). However, simulating complicated ocean-BGC interactions in an operational setting may not be computationally feasible for many modeling centers. Instead, the model-analog technique could provide an efficient alternative should high-resolution climate data libraries featuring BGC output become available.

CRediT authorship contribution statement

Dillon J. Amaya: Writing – review & editing, Writing – original draft, Visualization, Validation, Supervision, Software, Resources, Project administration, Methodology, Investigation, Formal analysis, Data curation, Conceptualization. **Michael G. Jacox:** Writing – review & editing, Methodology, Conceptualization. **Michael A. Alexander:** Writing – review & editing, Methodology, Conceptualization.

Declaration of competing interest

The authors declare that they have no known competing financial interests or personal relationships that could have appeared to influence the work reported in this paper.

Acknowledgements

We thank Jon Beverly and three anonymous reviewers for their helpful comments and suggestions, which improved the quality of this manuscript. This work was supported by the NOAA MAPP program.

Data availability

Data will be made available on request.

References

Abrahms, B., Welch, H., Brodie, S., Jacox, M.G., Becker, E.A., Bograd, S.J., Irvine, L.M., Palacios, D.M., Mate, B.R., Hazen, E.L., 2019. Dynamic ensemble models to predict distributions and anthropogenic risk exposure for highly mobile species. Divers. Distrib. 25, 1182–1193. https://doi.org/10.1111/ddi.12940.

Alexander, M.A., Bladé, I., Newman, M., Lanzante, J.R., Lau, N.C., Scott, J.D., 2002. The atmospheric bridge: the influence of ENSO teleconnections on air-sea interaction over the global oceans. J. Clim. 15, 2205–2231. https://doi.org/10.1175/1520-0442(2002)015%253C2205:TABTIO%253E2.0.CO;2.

Alexander, M.A., Scott, J.D., Friedland, K.D., Mills, K.E., Nye, J.A., Pershing, A.J., Thomas, A.C., 2018. Projected sea surface temperatures over the 21st century: changes in the mean, variability and extremes for large marine ecosystem regions of Northern Oceans. Elem. Sci. Anth. 6, 9. https://doi.org/10.1525/elementa.191.

Alexander, M.A., Scott, J.D., Jacox, M.G., Amaya, D.J., Wilczynski, L.M., 2025. Processes that Influence Bottom Temperatures in the California Current System. J. Geophys. Res. Oceans 130, e2024JC021886. https://doi.org/10.1029/2024JC021886.

Alexander, M.A., Scott, J.D., Jacox, M.G., Deser, C., Amaya, D.J., Capotondi, A., Phillips, A.S., 2023. A survey of coastal conditions around the continental US using a high-resolution ocean reanalysis. Prog. Oceanogr. 216, 103055. https://doi.org/10.1016/j.pocean.2023.103055.

Amaya, D.J., Alexander, M.A., Scott, J.D., Jacox, M.G., 2023. An evaluation of high-resolution ocean reanalyses in the California current system. Prog. Oceanogr. 210, 102951. https://doi.org/10.1016/j.pocean.2022.102951.

Amaya, D.J., Jacox, M.G., Alexander, M.A., Bograd, S.J., Jia, L., 2024. Seasonal Upwelling forecasts in the California Current System. Geophys. Res. Lett. 51, e2024GL111083. https://doi.org/10.1029/2024GL111083.

Amaya, D.J., Jacox, M.G., Dias, J., Alexander, M.A., Karnauskas, K.B., Scott, J.D., Gehne, M., 2022. Subseasonal-to-Seasonal Forecast Skill in the California Current System and its connection to Coastal Kelvin Waves. J. Geophys. Res. Oceans 127, e2021JC017892. https://doi.org/10.1029/2021JC017892.

Anderson, C.R., Berdalet, E., Kudela, R.M., Cusack, C.K., Silke, J., O'Rourke, E., Dugan, D., McCammon, M., Newton, J.A., Moore, S.K., Paige, K., Ruberg, S., Morrison, J.R., Kirkpatrick, B., Hubbard, K., Morell, J., 2019. Scaling up from Regional Case Studies to a Global Harmful Algal Bloom observing System. Front. Mar. Sci. 6. https://doi.org/10.3389/fmars.2019.00250.

Becker, E.J., Kirtman, B.P., L'Heureux, M., Muñoz, Á.G., Pegion, K., 2022. A Decade of the north American Multimodel Ensemble (NMME): Research, Application, and Future Directions. Bull. Am. Meteorol. Soc. 103, E973–E995. https://doi.org/10.1175/BAMS-D-20-0327.1.

Brodie, S., Jacox, M.G., Bograd, S.J., Welch, H., Dewar, H., Scales, K.L., Maxwell, S.M., Briscoe, D.M., Edwards, C.A., Crowder, L.B., Lewison, R.L., Hazen, E.L., 2018. Integrating Dynamic Subsurface Habitat Metrics into Species distribution Models. Front. Mar. Sci. 5. https://doi.org/10.3389/fmars.2018.00219.

Brodie, S., Pozo Buil, M., Welch, H., Bograd, S.J., Hazen, E.L., Santora, J.A., Seary, R., Schroeder, I.D., Jacox, M.G., 2023. Ecological forecasts for marine resource management during climate extremes. Nat. Commun. 14, 7701. https://doi.org/10.1038/s41467-023-43188-0.

Cannizzo, Z.J., Selz, V., 2021. National Marine Sanctuary Climate Change Science Priorities Workshop Report. https://doi.org/10.25923/4FTJ-3F44.

Chang, P., Xu, G., Kurian, J., Small, R.J., Danabasoglu, G., Yeager, S., Castruccio, F., Zhang, Q., Rosenbloom, N., Chapman, P., 2023. Uncertain future of sustainable fisheries environment in eastern boundary upwelling zones under climate change. Commun. Earth Environ. 4, 1–9. https://doi.org/10.1038/s43247-023-00681-0.

Chang, P., Zhang, S., Danabasoglu, G., Yeager, S.G., Fu, H., Wang, H., Castruccio, F.S., Chen, Y., Edwards, J., Fu, D., Jia, Y., Laurindo, L.C., Liu, X., Rosenbloom, N., Small, R.J., Xu, G., Zeng, Y., Zhang, Q., Bacmeister, J., Bailey, D.A., Duan, X., DuVivier, A.K., Li, D., Li, Y., Neale, R., Stössel, A., Wang, L., Zhuang, Y., Baker, A., Bates, S., Dennis, J., Diao, X., Gan, B., Gopal, A., Jia, D., Jing, Z., Ma, X., Saravanan, R., Strand, W.G., Tao, J., Yang, H., Wang, X., Wei, Z., Wu, L., 2020. An Unprecedented Set of High-Resolution Earth System Simulations for Understanding Multiscale Interactions in climate Variability and Change. J. Adv. Model. Earth Syst. 12, e2020MS002298. https://doi.org/10.1029/2020MS002298.

Chavez, F.P., Messié, M., 2009. A comparison of Eastern Boundary Upwelling Ecosystems. Prog. Oceanogr. 83, 80–96. https://doi.org/10.1016/j.pocean.2009.07.032.

Cimino, M.A., Santora, J.A., Schroeder, I., Sydeman, W., Jacox, M.G., Hazen, E.L., Bograd, S.J., 2020. Essential krill species habitat resolved by seasonal upwelling and ocean circulation models within the large marine ecosystem of the California Current System. Ecography 43, 1536–1549. https://doi.org/10.1111/ecog.05204.

Ding, H., Alexander, M.A., 2023. Multi-Year Predictability of Global Sea Surface Temperature using Model-Analogs. Geophys. Res. Lett. 50, e2023GL104097. https://doi.org/10.1029/2023GL104097.

Ding, H., Newman, M., Alexander, M.A., Wittenberg, A.T., 2019. Diagnosing Secular Variations in Retrospective ENSO Seasonal Forecast Skill using CMIP5 Model-Analogs. Geophys. Res. Lett. 46, 1721–1730. https://doi.org/10.1029/2018GL080598.

Ding, H., Newman, M., Alexander, M.A., Wittenberg, A.T., 2018. Skillful climate forecasts of the Tropical Indo-Pacific Ocean using Model-Analogs. J. Clim. 31, 5437–5459. https://doi.org/10.1175/JCLI-D-17-0661.1.

Drenkard, E.J., Stock, C., Ross, A.C., Dixon, K.W., Adcroft, A., Alexander, M., Balaji, V., Bograd, S.J., Butenschön, M., Cheng, W., Curchitser, E., Lorenzo, E.D., Dussin, R., Haynie, A.C., Harrison, M., Hermann, A., Hollowed, A., Holsman, K., Holt, J., Jacox, M.G., Jang, C.J., Kearney, K.A., Muhling, B.A., Buil, M.P., Saba, V., Sandø, A. B., Tommasi, D., Wang, M., 2021. Next-generation regional ocean projections for living marine resource management in a changing climate. ICES J. Mar. Sci. 78, 1969–1987. https://doi.org/10.1093/icesjms/fsab100.

Huang, B., Liu, C., Banzon, V., Freeman, E., Graham, G., Hankins, B., Smith, T., Zhang, H. M., 2021. Improvements of the Daily Optimum Interpolation Sea Surface Temperature (DOISST) Version 2.1. J. Clim. 34, 2923–2939. https://doi.org/10.1175/JCLI-D-20-0166.1.

Infanti, J.M., Kirtman, B.P., 2019. A comparison of CCSM4 high-resolution and low-resolution predictions for south Florida and southeast United States drought. Clim. Dyn. 52, 6877–6892. https://doi.org/10.1007/s00382-018-4553-0.

Jacox, M.G., Alexander, M.A., Mantua, N.J., Scott, J.D., Hervieux, G., Webb, R.S., Werner, F.E., 2018. Forcing of multiyear extreme ocean temperatures that impacted California current living marine resources in 2016. Bull. Am. Meteorol. Soc. 99, S27–S33. https://doi.org/10.1175/BAMS-D-17-0119.1.

Jacox, M.G., Alexander, M.A., Siedlecki, S., Chen, K., Kwon, Y.O., Brodie, S., Ortiz, I., Tommasi, D., Widlansky, M.J., Barrie, D., Capotondi, A., Cheng, W., Di Lorenzo, E., Edwards, C., Fiechter, J., Fratantoni, P., Hazen, E.L., Hermann, A.J., Kumar, A., Miller, A.J., Pirhalla, D., Pozo Buil, M., Ray, S., Sheridan, S.C., Subramanian, A., Thompson, P., Thorne, L., Annamalai, H., Aydin, K., Bograd, S.J., Griffis, R.B., Kearney, K., Kim, H., Mariotti, A., Merrifield, M., Rykaczewski, R., 2020. Seasonal-to-interannual prediction of north American coastal marine ecosystems: Forecast methods, mechanisms of predictability, and priority developments. Prog. Oceanogr. 183. https://doi.org/10.1016/j.pocean.2020.102307.

Jacox, M.G., Buil, M.P., Brodie, S., Alexander, M.A., Amaya, D.J., Bograd, S.J., Edwards, C.A., Fiechter, J., Hazen, E.L., Hervieux, G., Tommasi, D., 2023. Downscaled seasonal forecasts for the California Current System: Skill assessment and prospects for living marine resource applications. PLOS Clim. 2, e0000245. https://doi.org/10.1371/journal.pclm.0000245.

Jacox, M.G., Fiechter, J., Moore, A.M., Edwards, C.A., 2015. ENSO and the California current coastal upwelling response. J. Geophys. Res. Oceans 120, 1691–1702. https://doi.org/10.1002/2014JC010650.

Kearney, K.A., Alexander, M., Aydin, K., Cheng, W., Hermann, A.J., Hervieux, G., Ortiz, I., 2021. Seasonal Predictability of Sea Ice and Bottom Temperature across the Eastern Bering Sea Shelf. J. Geophys. Res. Oceans 126, e2021JC017545. https://doi.org/10.1029/2021JC017545.

Kim, W.M., Yeager, S.G., Danabasoglu, G., Chang, P., 2023. Exceptional multi-year prediction skill of the Kuroshio Extension in the CESM high-resolution decadal prediction system. npj Clim. Atmos. Sci. 6, 1–14. https://doi.org/10.1038/s41612-023-00444-w.

Lellouche, J.-M., Greiner, E., Bourdallé Badie, R., Garric, G., Melet, A., Drévillon, M., Bricaud, C., Hamon, M., Le Galloudec, O., Regnier, C., Candela, T., Testut, C.-E., Gasparin, F., Ruggiero, G., Benkiran, M., Drillet, Y., Le Traon, P.-Y., 2021. The Copernicus Global 1/12° Oceanic and Sea Ice GLORYS12 Reanalysis. Front. Earth Sci. 9. https://doi.org/10.3389/feart.2021.698876.

Lin, M., Horowitz, L.W., Zhao, M., Harris, L., Ginoux, P., Dunne, J., Malyshev, S., Shevliakova, E., Ahsan, H., Garner, S., Paulot, F., Pouyaei, A., Smith, S.J., Xie, Y., Zadeh, N., Zhou, L., 2024. The GFDL Variable-Resolution Global Chemistry-climate Model for Research at the Nexus of US climate and Air Quality Extremes. J. Adv. Model. Earth Syst. 16, e2023MS003984. https://doi.org/10.1029/2023MS003984.

Little, C.M., Yeager, S.G., Ponte, R.M., Chang, P., Kim, W.M., 2024. Influence of Ocean Model Horizontal Resolution on the Representation of Global Annual-To-Multidecadal Coastal Sea Level Variability. Journal of Geophysical Research: Oceans Lit e2024JC021679. https://doi.org/10.1029/2024JC021679.

Lorenz, E.N., 1969. Atmospheric Predictability as Revealed by naturally Occurring Analogues. J. Atmos. Sci. 26, 636–646. https://doi.org/10.1175/1520-0469(1969)26%253C636:APARBN%253E2.0.CO;2.

Lou, J., Joh, Y., Delworth, T.L., Jia, L., 2025. Identifying source of predictability for vapor pressure deficit variability in the southwestern United States. npj Clim. Atmos. Sci. 8, 1–14. https://doi.org/10.1038/s41612-025-01028-6.

Lou, J., Newman, M., Hoell, A., 2023. Multi-decadal variation of ENSO forecast skill since the late 1800s. npj Clim. Atmos. Sci. 6, 1–14. https://doi.org/10.1038/s41612-023-00417-z.

Meehl, G.A., Yang, D., Arblaster, J.M., Bates, S.C., Rosenbloom, N., Neale, R., Bacmeister, J., Lauritzen, P.H., Bryan, F., Small, J., Truesdale, J., Hannay, C., Shields, C., Strand, W.G., Dennis, J., Danabasoglu, G., 2019. Effects of Model Resolution, Physics, and Coupling on Southern Hemisphere storm Tracks in CESM1.3. Geophys. Res. Lett. 46, 12408–12416. https://doi.org/10.1029/2019GL084057.

Menary, M.B., Mignot, J., Robson, J., 2021. Skilful decadal predictions of subpolar North Atlantic SSTs using CMIP model-analogues. Environ. Res. Lett. 16, 064090. https://doi.org/10.1088/1748-9326/ac06fb.

Minobe, S., Capotondi, A., Jacox, M.G., Nonaka, M., Rykaczewski, R.R., 2022. Toward Regional Marine Ecological forecasting using Global climate Model predictions from Subseasonal to Decadal Timescales: Bottlenecks and Recommendations. Front. Mar. Sci. 9. https://doi.org/10.3389/fmars.2022.855965.

Moore, A.M., Arango, H.G., Broquet, G., Powell, B.S., Weaver, A.T., Zavala-Garay, J., 2011. The Regional Ocean Modeling System (ROMS) 4-dimensional variational data assimilation systems. Part I - System overview and formulation. Prog. Oceanogr. 91, 34–49. https://doi.org/10.1016/j.pocean.2011.05.004.

Neveu, E., Moore, A.M., Edwards, C.A., Fiechter, J., Drake, P., Crawford, W.J., Jacox, M. G., Nuss, E., 2016. An historical analysis of the California current circulation using ROMS 4D-Var: System configuration and diagnostics. Ocean Model. 99, 133–151. https://doi.org/10.1016/j.ocemod.2015.11.012.

Rader, J.K., Barnes, E.A., 2023. Optimizing Seasonal-To-Decadal Analog forecasts with a Learned Spatially-Weighted Mask. Geophys. Res. Lett. 50, e2023GL104983. https://doi.org/10.1029/2023GL104983.

Reynolds, R.W., Smith, T.M., Liu, C., Chelton, D.B., Casey, K.S., Schlax, M.G., 2007. Daily high-resolution-blended analyses for sea surface temperature. J. Clim. https://doi.org/10.1175/2007JCLI1824.1.

Ross, A.C., Stock, C.A., Koul, V., Delworth, T.L., Lu, F., Wittenberg, A., Alexander, M.A., 2024. Dynamically downscaled seasonal ocean forecasts for north American east coast ecosystems. Ocean Sci. 20, 1631–1656. https://doi.org/10.5194/os-20-1631-2024.

Santora, J.A., Mantua, N.J., Schroeder, I.D., Field, J.C., Hazen, E.L., Bograd, S.J., Sydeman, W.J., Wells, B.K., Calambokidis, J., Saez, L., Lawson, D., Forney, K.A., 2020. Habitat compression and ecosystem shifts as potential links between marine heatwave and record whale entanglements. Nat. Commun. 11, 536. https://doi.org/10.1038/s41467-019-14215-w.

Schroeder, I.D., Santora, J.A., Mantua, N., Field, J.C., Wells, B.K., Hazen, E.L., Jacox, M., Bograd, S.J., 2022. Habitat compression indices for monitoring ocean conditions and ecosystem impacts within coastal upwelling systems. Ecol. Ind. 144, 109520. https://doi.org/10.1016/j.ecolind.2022.109520.

Siedlecki, S.A., Kaplan, I.C., Hermann, A.J., Nguyen, T.T., Bond, N.A., Newton, J.A., Williams, G.D., Peterson, W.T., Alin, S.R., Feely, R.A., 2016. Experiments with Seasonal forecasts of ocean conditions for the Northern region of the California current upwelling system. Sci. Rep. 6. https://doi.org/10.1038/srep27203.

Siqueira, L., Kirtman, B.P., Laurindo, L.C., 2021. Forecasting Remote Atmospheric Responses to Decadal Kuroshio Stability Transitions. https://doi.org/10.1175/JCLI-D-20-0139.1.

Small, R.J., Kurian, J., Chang, P., Xu, G., Tsujino, H., Yeager, S., Danabasoglu, G., Kim, W.M., Altuntas, A., Castruccio, F., 2024. Eastern Boundary Upwelling Systems in Ocean–Sea Ice Simulations Forced by CORE and JRA55-do: Mean State and Variability at the Surface. Doi: 10.1175/JCLI-D-23-0511.1.

Tommasi, D., Stock, C.A., Hobday, A.J., Methot, R., Kaplan, I.C., Eveson, J.P., Holsman, K., Miller, T.J., Gaichas, S., Gehlen, M., Pershing, A., Vecchi, G.A., Msadek, R., Delworth, T., Eakin, C.M., Haltuch, M.A., Séférian, R., Spillman, C.M., Hartog, J.R., Siedlecki, S., Samhouri, J.F., Muhling, B., Asch, R.G., Pinsky, M.L., Saba, V.S., Kapnick, S.B., Gaitan, C.F., Rykaczewski, R.R., Alexander, M.A., Xue, Y., Pegion, K.V., Lynch, P., Payne, M.R., Kristiansen, T., Lehodey, P., Werner, F.E., 2017. Managing living marine resources in a dynamic environment: the role of seasonal to decadal climate forecasts. Prog. Oceanogr. 152, 15–49. https://doi.org/10.1016/j.pocean.2016.12.011.

Toride, K., Newman, M., Hoell, A., Capotondi, A., Schlör, J., Amaya, D.J., 2025. Using Deep Learning to Identify Initial Error Sensitivity for Interpretable ENSO Forecasts. https://doi.org/10.1175/AIES-D-24-0045.1.

Welch, H., Hazen, E.L., Briscoe, D.K., Bograd, S.J., Jacox, M.G., Eguchi, T., Benson, S.R., Fahy, C.C., Garfield, T., Robinson, D., Seminoff, J.A., Bailey, H., 2019. Environmental indicators to reduce loggerhead turtle bycatch offshore of Southern California. Ecol. Ind. 98, 657–664. https://doi.org/10.1016/j.ecolind.2018.11.001.

Wills, R.C.J., Herrington, A.R., Simpson, I.R., Battisti, D.S., 2024. Resolving Weather Fronts increases the Large-Scale Circulation Response to Gulf Stream SST Anomalies in Variable-Resolution CESM2 Simulations. J. Adv. Model. Earth Syst. 16, e2023MS004123. https://doi.org/10.1029/2023MS004123.

Xu, T., Newman, M., Alexander, M.A., Capotondi, A., 2024. Seasonal Predictability of Bottom Temperatures along the north American West Coast. J. Geophys. Res. Oceans 129, e2023JC020504. https://doi.org/10.1029/2023JC020504.

Yeager, S.G., Chang, P., Danabasoglu, G., Rosenbloom, N., Zhang, Q., Castruccio, F.S., Gopal, A., Cameron Rencurrel, M., Simpson, I.R., 2023. Reduced Southern Ocean warming enhances global skill and signal-to-noise in an eddy-resolving decadal prediction system. npj Clim. Atmos. Sci. 6, 1–13. https://doi.org/10.1038/s41612-023-00434-y.

Zhang, Q., Chang, P., Fu, D., Yeager, S.G., Danabasoglu, G., Castruccio, F., Rosenbloom, N., 2024. Enhanced Atlantic Meridional Mode predictability in a high-resolution prediction system. Sci. Adv. 10, eado6298. https://doi.org/10.1126/sciadv.ado6298.

Zhang, S., Fu, H., Wu, L., Li, Y., Wang, H., Zeng, Y., Duan, X., Wan, W., Wang, L.i., Zhuang, Y., Meng, H., Xu, K., Xu, P., Gan, L., Liu, Z., Wu, S., Chen, Y., Yu, H., Shi, S., Wang, L., Xu, S., Xue, W., Liu, W., Guo, Q., Zhang, J., Zhu, G., Tu, Y., Edwards, J., Baker, A., Yong, J., Yuan, M., Yu, Y., Zhang, Q., Liu, Z., Li, M., Jia, D., Yang, G., Wei, Z., Pan, J., Chang, P., Danabasoglu, G., Yeager, S., Rosenbloom, N., Guo, Y., 2020. Optimizing high-resolution Community Earth System Model on a heterogeneous many-core supercomputing platform. Geosci. Model Dev. 13, 4809–4829. https://doi.org/10.5194/gmd-13-4809-2020.